

The 3'-5' exoribonuclease Dis3 regulates the expression of specific microRNAs in Drosophila wing imaginal discs

Article (Accepted Version)

Towler, Benjamin P, Jones, Christopher I, Viegas, Sandra C, Apura, Patricia, Waldron, Joseph A, Smalley, Sarah K, Arraiano, Cecilia M and Newbury, Sarah F (2015) The 3'-5' exoribonuclease Dis3 regulates the expression of specific microRNAs in Drosophila wing imaginal discs. *RNA Biology*, 12 (7). pp. 728-741. ISSN 1547-6286

This version is available from Sussex Research Online: <http://sro.sussex.ac.uk/id/eprint/53661/>

This document is made available in accordance with publisher policies and may differ from the published version or from the version of record. If you wish to cite this item you are advised to consult the publisher's version. Please see the URL above for details on accessing the published version.

Copyright and reuse:

Sussex Research Online is a digital repository of the research output of the University.

Copyright and all moral rights to the version of the paper presented here belong to the individual author(s) and/or other copyright owners. To the extent reasonable and practicable, the material made available in SRO has been checked for eligibility before being made available.

Copies of full text items generally can be reproduced, displayed or performed and given to third parties in any format or medium for personal research or study, educational, or not-for-profit purposes without prior permission or charge, provided that the authors, title and full bibliographic details are credited, a hyperlink and/or URL is given for the original metadata page and the content is not changed in any way.

The 3'-5' exonuclease Dis3 regulates the expression of specific microRNAs in *Drosophila* wing imaginal discs.

Benjamin P. Towler¹, Christopher I. Jones^{1*}, Sandra C. Viegas^{2*}, Patricia Apura², Joseph A. Waldron¹, Sarah K. Smalley, Cecilia M. Arraiano² and Sarah F. Newbury^{1*}.

¹ Brighton and Sussex Medical School, Medical Research Building, University of Sussex, Falmer, Brighton, BN1 9PS, UK.

² Instituto de Tecnologia Química e Biológica, Universidade Nova de Lisboa, Av. da República, 2780-157 Oeiras, Portugal.

*Corresponding author: s.newbury@bsms.ac.uk +44 (0)1273 877874.

+ These authors contributed equally to this work.

Key words

Dis3/Taz, RNA stability, RNA degradation, *Drosophila* development, imaginal discs, miRNAs, exonuclease.

Abstract

Dis3 is a highly conserved exoribonuclease which degrades RNAs in the 3'-5' direction. Mutations in Dis3 are associated with a number of human cancers including multiple myeloma and acute myeloid leukaemia. In this work, we have assessed the effect of a Dis3 knockdown on *Drosophila* imaginal disc development and on expression of mature microRNAs. We find that Dis3 knockdown severely disrupts the development of wing imaginal discs in that the flies have a "no wing" phenotype. Use of RNA-seq to quantify the effect of Dis3 knockdown on microRNA expression shows that Dis3 normally regulates a small subset of microRNAs, with only 11 (10.1%) increasing in level ≥ 2 -fold and 6 (5.5%) decreasing in level ≥ 2 -fold. Of these microRNAs, *miR-252-5p* is increased 2.1-fold in Dis3-depleted cells compared to controls while the level of the *miR-252* precursor is unchanged, suggesting that Dis3 can act in the cytoplasm to specifically degrade this mature miRNA. Furthermore, our experiments suggest that Dis3 normally interacts with the exosomal subunit Rrp40 in the cytoplasm to target *miR-252-5p* for degradation during normal wing development. Another microRNA, *miR-982-5p*, is expressed at lower levels in Dis3 knockdown cells, while the *miR-982* precursor remains unchanged, indicating that Dis3 is involved in its processing. Our study therefore reveals an unexpected specificity for this ribonuclease towards microRNA regulation, which is likely to be conserved in other eukaryotes and may be relevant to understanding its role in human disease.

Introduction

Ribonucleases are enzymes that degrade or process RNAs. Since the level of a particular RNA within a cell is the result of a balance between RNA synthesis and degradation, ribonucleases are key components in the regulation of gene expression. There is increasing evidence that mutations in genes encoding ribonucleases can result in defects in cellular processes, organism viability and cancer, suggesting that they play a key role in development and differentiation.¹⁻⁴ Furthermore, recent data has shown that ribonucleases can target specific RNAs, which can in turn affect specific cellular pathways.^{5,6} However, the effects of ribonucleases on biological functions and the RNAs targeted by specific ribonucleases in whole organisms or tissues are not well understood.

This paper focuses on Dis3/Tazman, a highly processive ribonuclease that belongs to the RNaseII/RNB family of hydrolytic 3'-5' exonucleases.⁷ In the yeast *S. cerevisiae*, only one form of Rrp44/Dis3 is present, whereas there are two paralogues present in *Drosophila melanogaster* (*Dis3* and *Dis3L2*) and three in humans (*DIS3*, *DIS3L1* and *DIS3L2*).^{3,8} Dis3 and Dis3L1 are known to associate with the exosome, a nine-subunit core complex which serves to channel the RNA through its central core to the catalytic subunit.⁹⁻¹² In eukaryotes, Dis3 proteins are similar in domain structure and include a CR3 motif, two cold-shock (OB) domains, the RNB domain, an S1 domain and two putative nuclear localisation sequences. The cold-shock domains and S1 domains are ancient folds that non-specifically bind RNA, while the exonucleolytic activity is provided by the RNB domain. Dis3 and Dis3L1 also include a PIN (PiIT N-terminus) domain located at the N-terminus between the CR3 motif and the cold-shock domains. The PIN domain in Dis3 is known to catalyse endonucleolytic RNA decay as well as tethering Dis3 to the exosome.¹³ Although Dis3L1 includes a PIN domain which results in its association with the core exosome, this PIN domain does not have endonucleolytic activity.^{11, 14, 15} Dis3L2 has a similar domain structure to Dis3 and Dis3L1 but does not include a PIN domain, does not associate with the exosome and is responsible for an alternative degradation pathway involving uridylation of RNA substrates.^{8, 16-18} Previous reports using human and *Drosophila* tissue culture cells or *Drosophila* oocytes have shown that Dis3 is predominantly located in the nucleus but is also present in the cytoplasm.^{7, 11, 19, 20} In human tissue culture cells DIS3L1 and DIS3L2 are restricted to the cytoplasm.^{8, 11, 12, 17}

Dis3 has essential functions in the cell as null mutations result in lethality.²¹⁻²⁴ Loss of function by hypomorphic mutations or by RNA knockdown using siRNAs also results in reduced cell survival.²⁴ Global screens have revealed that mutations or aberrant expression of Dis3 are often associated with human cancers such as multiple myeloma, medulloblastoma, acute myeloid leukaemia and melanoma.²⁵⁻²⁸ The effects of Dis3 on cell survival and proliferation are most likely due to increased amounts of target RNAs which, directly or indirectly, perturb cellular functions. The reported targets of Dis3 reflect its predominantly nuclear location and include human PROMPTS (promoter upstream transcripts) or yeast CUTs (cryptic unstable transcripts), excised introns, pre-mRNAs and pre-tRNAs as well as snRNAs and snoRNAs.^{22, 24, 29} Dis3 also plays a role in microRNA (miRNA) biogenesis, in that it is also involved in the maturation of miRNAs derived from introns (mirtrons) such as *Drosophila* *miR-1017* and the trimming of pre-miRNA 3' ends.³⁰ In *Drosophila* S2 cells, depletion of Dis3 using RNA interference results in increases in RNAs encoding cell cycle related proteins, whereas in whole larvae, Dis3 knockdown results in the increase of a discrete set of transcripts at different stages of development.^{31, 32} However, the effect of Dis3 on the development of a specific tissue or on mature miRNAs in whole organisms has not yet been addressed.

In this paper, we have, for the first time, used genome-wide profiling (miRNA-seq) on *Drosophila* wing imaginal discs to assess the effect of Dis3 on mature miRNA gene expression. We show that Dis3 knockdown within wing imaginal discs has a profound effect on wing differentiation and on developmental timing. We also show that, surprisingly, Dis3 knockdown affects the levels of a small set of miRNAs, whereas the levels of most miRNAs are unaffected. For one miRNA, the levels of mature miRNA increase whilst the levels of its precursor remain unchanged, suggesting that Dis3 is involved in the degradation of this miRNA in the cytoplasm.

Results

Knockdown of Dis3 in the wing imaginal discs results in severe wing defects and delayed development.

In order to determine the effect of Dis3/Taz on miRNA expression in imaginal discs, we first analysed the effect of Dis3 depletion on development of this tissue. As expected, knockdown of Dis3 using ubiquitous GAL4 drivers and *UAS-Dis3^{RNAi}* results in complete lethality at or prior to the L2 larval

stage (**Table 1**). Knockdown of Dis3 over the entire wing imaginal disc using the *69B-GAL4* driver also results in lethality at the L2 or L3 stage (**Table 1**). However, restricting knockdown of Dis3 to the wing pouch area of the disc, using the *nubbin-GAL4* driver, results in a severe "no wing" phenotype where there is a complete absence of wing blade development (100% penetrance) (**Fig. 1, panels A and B**). In addition to the absence of wing development, late L3 imaginal discs were 77% the size of parental control discs (**Fig. 2, panels A - C**). Staining with Anti-activated Caspase 3 indicates extensive apoptosis specifically in the region of Dis3 depletion (**Fig. 2, panels D-E**). This result indicates that Dis3 is required for viability of cells within the wing pouch and also provides an explanation for the reduced area of the wing imaginal discs. Abnormal haltere development was also observed (**Fig. 1, panels D - E**) as *nubbin-GAL4* also drives expression in these discs.³³ Although knockdown of Dis3 in the wing pouch (**Fig. 1, panel C**) does not result in lethality, the *nubbin-GAL4; UAS-Dis3^{RNAi}* flies were delayed in larval development by 40 hours at 25°C (**Fig. 1, panel F**). In agreement with these results, knockdown of Dis3 using the *pannier-GAL4* driver to drive expression in tip of the wing disc, which goes on to form the dorsal part of the thorax, results in a severe cleft thorax phenotype (penetrance 100%) (**Supplemental Fig. 1**). These experiments show that Dis3 is essential for the development of wing imaginal discs into wing and thoracic tissues.

Global miRNA profiling experiments using RNA-seq reveal that a small subset of specific miRNAs changes in expression upon Dis3 depletion.

To determine the effect of Dis3 on miRNA expression in the wing imaginal disc we used the *nubbin-GAL4* driver together with *UAS-Dis3^{RNAi}* as the limited knockdown of Dis3 in the wing pouch provides a strong phenotype and also suitable tissue for collection for global miRNA profiling. Controls comprised the two parental stocks used to generate the Dis3 knockdown flies (*;nub-GAL4*; and *;UAS-Dis3^{RNAi}*). Knockdown of *dis3* RNA, using this shRNA system, resulted in 80% knockdown at the protein level within wing imaginal discs (**Fig. 1, panel C**), even though knockdown only occurs in the wing pouch region of the disc. Total RNA was prepared from two biological replicates of 60 wing imaginal discs per genotype and sent to ARK genomics, Roslin Institute, Edinburgh for small library preparation and RNA-sequencing. The sequencing output was mapped to miRBase release 19 to identify the known miRNAs present within each sample.

Of the 426 previously annotated miRNAs in *Drosophila* (miRBase 19), 109 were detected that had >1 read in all samples. Duplicates of each sample clustered together (indicating similar miRNA expression profiles) whilst the two parental samples were more similar to each other than they are to the knockdown samples (**Supplemental Fig. 2**). Expression of 101 (92.7%) miRNAs, normalised to the total number of reads, were similar between parental stocks; those miRNAs that differed more than 2-fold between the parental genotypes were removed from the analysis. To investigate how the levels of each miRNA changed in expression upon Dis3 depletion, the number of reads per miRNA were normalised to the total number of aligned reads within the sample (RPKM). The normalised read count was then compared between control and knockdown samples. Interestingly, the overall expression profiles of miRNAs in wing discs show a bimodal distribution with the highly expressed group (**Fig. 3, panel A**; right hand peak) showing 100 times greater expression than the lowly expressed group (left hand peak). Overall, 67 (61.5%) miRNAs did not change in expression between knockdown and control samples showing that Dis3 depletion does not result in global increases or decreases in miRNA levels (**Fig. 3, panels B and E**). Depletion of Dis3 results in changes in expression of a subset of miRNAs, with 29 (26.6%) increasing ≥ 1.5 -fold and 13 (11.9%) decreasing ≥ 1.5 -fold. These data also show that knockdown of Dis3 affects the expression of poorly expressed miRNAs more than that of highly expressed miRNAs (**Fig 3, panels A and D**), suggesting that Dis3 is normally involved in maintaining these miRNAs at low levels. Dis3 could act on these miRNAs either directly (e.g. by degradation of the miRNA by Dis3) or indirectly (e.g. by control of an mRNA target that subsequently affects the levels of one or more miRNAs).

We have previously published information on the abundance of miRNAs in wing imaginal discs obtained from microarray analysis.⁵ We are now presenting, for the first time, data showing the abundance of miRNAs in wing imaginal discs using the more sensitive and unbiased RNA-seq analysis (**Supplemental Fig. 3**). A total of 109 mature miRNAs were detected (with >1 read per sample), with the most abundant miRNA, *miR-9a-5p*, roughly 12,000-fold more abundant than the levels of the least abundant miRNA reliably detected (*miR-307a-3p*). These results are similar to that of our previous study using microarrays⁵ in that the highly expressed miRNAs according to microarray analysis are also found to be most abundant in the more sensitive RNA-seq analysis. This analysis also confirms that the miRNAs that change ≥ 2 -fold in levels upon Dis3 depletion are also those that

are normally expressed at low levels in wing imaginal discs, suggesting that Dis3 plays a role in keeping the levels of these miRNAs low under normal conditions (Supplemental Fig. 3).

The effect of Dis3 depletion on miRNA levels in wing imaginal discs is shown in **Figure 4**. These data demonstrate that 11 miRNAs are increased ≥ 2 -fold in levels (blue text). Of these, five miRNAs (*miR-987-5p*, *miR-277-3p*, *miR-958-3p*, *miR-956-3p*, *miR-252-5p*) were upregulated ≥ 4 -fold in Dis3-depleted discs. In contrast, six miRNAs were decreased ≥ 2 -fold in levels (red text) with no miRNA downregulated ≥ 4 -fold. The majority of miRNAs (92) show changes of ≤ 2 -fold upon Dis3 depletion. These data show that Dis3 normally represses the expression of a small subset of miRNAs and induces (directly or indirectly) the expression of even fewer miRNAs

RNA-seq data reveals a novel miRNA, which is conserved in the red flour beetle (*Tribolium castaneum*)

The power of RNA-seq is illustrated by our discovery of a new miRNA that is expressed in wing imaginal discs (**Fig. 5**). This miRNA was identified by use of the programme miRDeep2, which scans the RNA-seq data for sequences that map to predicted miRNA precursors that are able to be generated by Dicer cleavage during miRNA biogenesis.³⁴ The predicted precursor for this miRNA is located at 2R:14067655-2R:14067710, within the 5'UTR of CG5726. This novel miRNA is similar to *miR-3882-5p* in the red flour beetle (*Tribolium castaneum*; 3 mismatches, score 63, E-value 5.1) suggesting that this is a biologically relevant miRNA. We also validated the presence of this novel miRNA using TaqMan qRT-PCR using a custom designed assay. The assay showed strong detection of the miRNA sequence whilst no signal was observed in no RT controls. However, according to both the RNA-seq and TaqMan qRT-PCR experiments, this novel miRNA does not change significantly in levels in Dis3-depleted cells compared to parental controls.

Verification of RNA-seq results using quantitative RT-PCR.

In order to validate the changes in miRNA abundance in wing imaginal discs following Dis3 depletion, we employed quantitative RT-PCR to confirm the fold changes shown by RNA-seq. The first criterion for choosing this set of miRNAs were that they should include only those which showed changes in levels of ≥ 2 -fold in both knockdown samples versus all control replicates. The second criterion was

that the RNA-seq read counts should show consistency between the knockdown samples and between each of the parental control replicates (see Materials and Methods for further information).

Figure 6, panel A graphically represents the variation between replicates, as well as the abundance of miRNAs in terms of RPKM. Using this stringent filtering method, we identified six miRNAs whose expression increased ≥ 2 -fold in the knockdown samples compared to both parental controls (*miR-277-3p*, *miR-987-5p*, *miR-252-5p*, *miR-34-5p*, and *miR-7-3p* and *miR-317-5p*). Two miRNAs whose expression was reduced ≥ 2 -fold (*miR-982-5p* and *miR-9b-3p*) were also identified (**Fig. 4 and Fig. 6, panel A**). Two miRNAs, *bantam-3p* and *miR-92b-3p* were chosen as controls as their levels remained the same in knockdown and parental samples.

The changes in expression of these miRNAs in Dis3-depleted wing imaginal discs compared to parental controls were validated using TaqMan qRT-PCR with *snoR442* as a normalisation control. Expression of each miRNA was tested in at least three biological replicates with four technical replicates in total per biological replicate (see Materials and Methods). **Figure 6, panel B** shows that the changes in expression levels for all selected miRNAs, as measured by qRT-PCR, were comparable with the levels determined by RNA-seq, apart from for *miR-7-3p* which had a very low normalised read count. The two control miRNAs, *bantam-3p* and *miR-92b-3p*, whose expression levels remained consistent across all samples according to RNA-seq data, also showed no significant changes as determined by qRT-PCR. Therefore, these data show that the changes in abundance of miRNAs upon Dis3 depletion, as measured by qRT-PCR, are similar to those determined by RNA-seq.

Mature *miR-252-5p* is a potential target for specific Dis3 degradation.

If miRNAs increase in expression in Dis3 knockdown cells then this could be due to the miRNA normally being targeted for degradation by Dis3. Alternatively, upregulation of the level of a miRNA could be a result of Dis3 knockdown indirectly upregulating the transcription of that miRNA. To test this we designed TaqMan primers specific to each of the pri/pre-miRNA precursors for each upregulated miRNA and compared the expression with that of mature miRNAs. Mature *miR-252-5p* appears to be a potential target of Dis3 because the levels of the *pri/pre-miR-252* precursor are similar in Dis3-depleted cells and controls whereas the mature *miR-252-5p* levels are 2.1-fold higher in

depleted cells compared to controls (by qRT-PCR; **Fig. 6, panel C**). In contrast, the levels of the pri/pre-miRNAs are increased in levels in Dis3-depleted cells for *miR-277-3p*, *miR-34-5p*, *miR-317-5p* and *miR-987-5p* suggesting that these miRNAs are not direct targets of Dis3.

Levels of *pre-miR-982-5p* are similar in Dis3-depleted cells compared to controls whereas the mature *miR-982-5p* decreases 4.4-fold (by qRT-PCR). This suggests that Dis3 is involved in the processing of the mature *miR-982-5p* from the *pre-miR-982* precursor. For *miR-9b-3p*, the levels of *pre-miR-9b* show a similar decrease to that of the mature miRNA suggesting that this miRNA is indirectly regulated by Dis3, perhaps by indirectly affecting transcription.

Overexpression of *miR-252-5p* in the wing pouch results in severe wing defects

If Dis3 normally affects wing growth by repressing the expression of *miR-252-5p*, then we would expect that overexpression should result in similar phenotypes to knockdown of Dis3. To test this, we first overexpressed *UAS-miR-252* pre-miRNA under the control of the *tubulin-GAL4* promoter. Similarly to the Dis3 knockdown, this resulted in complete lethality (**Fig. 7, panel A**). We then overexpressed *UAS-miR-252* in the wing pouch using the *nubbin-GAL4* driver. As expected, mature *miR-252-5p* was highly expressed (1154-fold increase) in the wing imaginal discs of *nub-GAL4/UAS-miR-252* larvae (**Fig. 7, panel B**). Overexpression of *miR-252* resulted in a similar but less severe phenotype to that seen in surviving Dis3 knockdown flies (100% penetrance) (compare **Fig. 7, panels C and D** with **Fig. 1, panels A and B**). Therefore it is possible that Dis3 normally targets *miR-252-5p* to keep its expression at low levels and prevent it from inhibiting wing development.

Knockdown of Rrp40, an exosome subunit, results in upregulation of *miR-252-5p*.

In *Drosophila*, the exosome subunit Rrp40 has been shown to be predominantly localised to the cytoplasm.³⁵ To determine if this exosome subunit is involved in the degradation of *miR-252-5p*, or whether Dis3 acts independently of this exosome subunit, we knocked down Rrp40 in the wing pouch using the *nubbin-GAL4* driver. As can be seen in **Figure 8, panels A-B** this knockdown resulted in phenotypes similar to, but less severe than, phenotypes seen for Dis3 knockdown. In addition, the levels of mature *miR-252-5p* increased 2.5-fold, which is comparable to the 2.1-fold increase seen in

Dis3-depleted cells (**Fig. 8, panel C**). This result is consistent with Dis3 acting in a complex with Rrp40 in the control of the levels of *miR-252-5p* in the cytoplasm.

Discussion

In this study, we have used RNA-seq to investigate the effects of knockdown of the 3'-5' exonuclease Dis3 on the levels of miRNAs in *Drosophila* wing imaginal discs. We show that the expression of a small subset (17/109) are changed ≥ 2 -fold upon Dis3 depletion. For two of the miRNAs, the changes in abundances of the mature miRNAs are not accompanied by changes in the levels of the precursor miRNAs, suggesting regulation at the post-transcriptional level. For the upregulated mature miRNA, *miR-252-5p*, this suggests that Dis3 can selectively degrade this miRNA in the cytoplasm. For the downregulated miRNA, *miR-982-5p*, our data are consistent with a role of Dis3 in the processing of the miRNA from the pre-miRNA precursor. We also show that overexpression of *miR-252-5p* produces a similar phenotype to knockdown of Dis3, demonstrating that regulation of this miRNA is important in wing development. Knockdown of the predominantly cytoplasmic exosome subunit Rrp40 also results in an upregulation of *miR-252-5p* and a similar but less severe phenotype than Dis3 depletion, suggesting that the exosome is at least partially required for the activity of Dis3 over this miRNA. This study therefore reveals, for the first time, that Dis3 appears to have important biological roles in the processing of specific mature miRNAs in the cytoplasm.

The use of RNA-seq as an unbiased approach to detect miRNAs in wing imaginal discs has also allowed us to assess the abundance of individual miRNAs within wing imaginal discs (rather than all imaginal discs) from larvae at the L3 stage. Our data show that the most abundant miRNA, *miR-9a-5p*, is about 12,000-fold more abundant than the levels of the least abundant miRNA reliably detected (*miR-307a-3p*). The abundance profile of miRNAs is in line with the profile determined by microarrays,⁵ although more miRNAs are detected by the more sensitive RNA-seq technique, as expected. Analysis of the RNA-seq data also identified a novel *Drosophila* miRNA, which is conserved in the red flour beetle, *Tribolium castaneum*. This analysis also shows that the miRNAs which are upregulated upon Dis3 depletion tend to be poorly expressed in wild-type discs, suggesting that Dis3 is normally required to maintain these miRNAs at low levels, at least during this stage of development.

The set of miRNAs that increase ≥ 2 -fold; by RNA-seq upon Dis3 depletion are *miR-277-3p*, *miR-987-5p*, *miR-252-5p*, *miR-34-5p* and *miR-317-5p* (**Table 2**). For *miR-277-3p*, *miR-987-5p* and *miR-34-5p* their cognate miRNA precursors also increase upon Dis3 knockdown, suggesting that Dis3 normally affects their expression via indirect means, perhaps by increasing the expression of specific transcription factors. Details on the known biological functions of these miRNAs in *Drosophila* are given in **Table 2**. In contrast, the expression of *pre-miR-252* does not increase upon Dis3 knockdown whereas the mature miRNA increases by 2.1-fold (by qRT-PCR). This suggests that Dis3 normally degrades this miRNA in the cytoplasm. *miR-252* is conserved in all *Drosophila* species and also in invertebrates (**Table 2**) suggesting that it has important biological functions. Overexpression of *miR-252* in the wing pouch gives a similar, although weaker phenotype to Dis3 knockdown, which is expected if it is a target of Dis3. This data is consistent with previous results showing that ectopic expression of *miR-252* in the wing pouch using the *scalloped-Gal4* driver also induced strong wing phenotypes.³⁶ In addition, it has been reported that a severe wing phenotype is observed when *miR-252-5p* is overexpressed using the *MS1096-GAL4* driver.³⁷ Wing phenotypes are not always seen when miRNAs are overexpressed in the wing; for example, no phenotype is seen when *miR-34* is overexpressed using *MS1096-GAL4*.³⁷ No targets of *miR-252-5p* have been determined experimentally, but predicted targets include mRNAs important in developmental processes such as *ultrabithorax* and *smoothened* (http://www.targetscan.org/fly_12/).

Of all the miRNAs detected by RNA-seq in Dis3 depleted wing imaginal discs, only one, *miR-982-5p*, showed a decrease in level (-4.4-fold by qRT-PCR) while its precursor remained unchanged. These data suggest that Dis3 is involved in the processing of the mature miRNA from its precursor miRNA. Although the qRT-PCR primers cannot distinguish the pri-miRNA precursor from the pre-miRNA precursor, our RNA-seq data shows that the *miR-982-3p* reads decrease to a similar extent to the *miR-982-5p* reads. This data supports the suggestion that Dis3 is involved in processing the pre-miRNA precursor from the pri-miRNA precursor. The biological function of *miR-982-5p* is not known but ectopic expression of *pre-miR-982* in the wing pouch using the *scalloped-GAL4* driver has been shown to produce phenotypes consistent with a connection to Notch signalling.³⁶

The above mechanism of regulation relies on a percentage of Dis3 protein being located in the cytoplasm. Our previous published work on ovaries and embryos, and that of others using S2 cells, has shown that Dis3 is predominantly located in the nucleus^{7, 19, 20} with about 10% being located in the cytoplasm.¹⁹ Therefore, there would appear to be sufficient Dis3 in the cytoplasm to carry out the activities observed. Since the upregulation of *miR-252-5p* in Dis3-depleted cells is similar to that in Rrp40-depleted discs it is likely that it is acting together with the core exosome complex rather than acting independently or in sub-complexes.³² Rrp40 has been shown to be predominantly localised to the cytoplasm in *Drosophila*,³⁵ therefore this would be consistent with the cytoplasmic exosome being responsible for the degradation of *miR-252-5p*. The phenotypes resulting from Rrp40 knockdown are also similar to Dis3 knockdown which is also consistent with Dis3 acting together with the core exosome complex.

An interesting feature of our research is the co-ordinate regulation of two miRNAs by the 3'-5' and 5'-3' degradation pathways. *miR-277-3p* increases 3.8-fold (by qRT-PCR, **Fig. 6, panel C**) upon Dis3 knockdown, with this increase most likely to be due to an indirect effect on transcription. In contrast, in the hypomorphic *pcm*⁵ mutant, where activity of the 5'-3' exoribonuclease Pacman (Xrn1) is decreased, mature *miR-277-3p* is decreased in expression by 5.6-fold, while the level of *pre-miR-277-3p* remains unchanged.⁵ These data therefore suggest that both Pacman and Dis3 are required to maintain this miRNA at the correct level in the wing imaginal discs. Therefore the normal expression of *miR-277-3p* would be achieved through a balance between upregulation by Pacman (perhaps due to increased processing from precursors) and downregulation by Dis3 (most likely due to indirect transcriptional effects). A similar effect is seen for *miR-34-5p* although the changes in levels are not so pronounced. The exact mechanistic pathways whereby this is achieved remains to be determined.

What are the mechanisms by which *miR-252-5p* may be targeted to Dis3 for degradation? One possibility is that this miRNA is selectively uridylylated or adenylated at the 3' end to promote degradation by Dis3. Adenylation by Wispy has been clearly shown to result in decreased stability of *miR-312* in *Drosophila* cells³⁸, however, the exoribonuclease responsible for the degradation has not been determined. It is therefore possible that *miR-252-5p* is normally adenylated (or possibly uridylylated) at the 3' end by a nucleotidyl transferase to promote its degradation. It has also been

reported that *Drosophila* miRNAs may be modified by 3' trimming by the exonuclease Nibbler.³⁹ As well as enhancing/inhibiting exonuclease activity these 3' end modifications may alter affinity for binding proteins such as AGO in the RISC and so promote or prevent release of the miRNA from the protein complex. However, our RNA-seq data shows no clear evidence for uridylation, adenylation or 3' trimming of this miRNA. One reason for this is that the two bases 3' to the canonical mature *miR-252-5p* sequence, as encoded by the DNA sequence, are uridines. Therefore we cannot distinguish whether the first and/or second uridines at the 3' end of some of the reads are a result of post-transcriptional additions (i.e. non-templated) or are encoded by the DNA template (i.e. templated). Similarly, *miR-982-5p* also has a uridine encoded at the next nucleotide after the 3' end of the mature miRNA in the DNA sequence. In addition, size selection of RNAs for the RNA-seq ranged from 18-22nt therefore there is very little scope for detection of non-templated nucleotides at the 3' ends of the RNA reads. Another way to promote miRNA instability could be the binding of *miR-252-5p* to its mRNA targets or to long non-coding targets.^{40, 41}

Our data also suggest that Dis3 can specifically affect processing of *miR-982-5p* from its precursors. This specificity could be conferred by preferential binding of Dis3 to pre-miRNAs with >2nt 3' overhangs plus binding and co-operation with the terminal uridyl transferases TUT7 and TUT4 as occurs in human cells.²⁹ An alternative scenario is that *pre-miR-982* binds to particular RNA binding proteins (e.g. Loquacious (PACT in mammals)^{42, 43}) to enable trimming of the precursor by Dis3. If Dis3 is involved in the processing of *pre-miR-982* during its biogenesis then in the absence of Dis3 one may expect the level of precursor to increase. However, our data shows that *pre-miR-982* remains unchanged following Dis3 knockdown. The reasons for this may be twofold; firstly in the absence of Dis3, *pre-miR-982* may be signalled for degradation by another 3'-5' exoribonuclease, for example, by addition of uridyl residues to the 3' end and degradation by Dis3L2 in a similar manner to that observed during *let-7* biogenesis in mouse and human cells.^{16, 18} Alternatively Dis3 could function in the final trimming of *miR-982-5p* similar to the activity observed for Nibbler.^{39, 44} In this case the *pre-miR-982* would be processed as normal by Dicer and therefore no change in *pre-miR-982* levels would be expected. Our findings set the stage for further mechanistic studies to understand the specificity of Dis3 in the control of miRNAs biogenesis and degradation.

Materials and Methods

Fly stocks, crosses and phenotypic analyses.

Fly stocks were cultivated on standard media at 25°C in uncrowded conditions. All stocks used were obtained from the Bloomington stock centre unless otherwise stated. GAL4 drivers used were: *tub-GAL4* ($P\{w^{+mC}=tubP-GAL4\}LL7$ originally from stock 5138, $y^1 w^+$;; $P\{w^{+mC}=tubP-GAL4\}LL7/TM6b,GFP$), *da-GAL4* (stock 108252, w^{1118} , $P\{w^{mW.hs}Gal4-da.G32\}UH1$), *nub-GAL4* (stock 25754; $P\{UAS-Dcr-2.D\}1$, w^{1118} ; $P\{GawB\}nub-AC-62$), *69B-GAL4* (stock 1774; w^+ ;; $P\{GawB\}69B$) and *pnr-GAL4* (stock 25758, $P\{UAS-Dcr-2.D\}1$, w^{1118} ; $P\{GawB\}pnr^{MD237}/TM3$). *UAS-miR-252* was obtained from FlyORF (stock F002053, $M\{UAS-miR-252.S\}ZH-86Fb$). RNAi stocks were obtained from the Vienna Drosophila RNAi Centre. Stocks used were: *UAS-Dis3^{RNAi}* (stock v35090, w^{1118} ;; $P\{GD11917\}v35090$ and stock v108013, ; $P\{KK101473\}VIE-260B$; , *UAS-Rrp40^{RNAi}* (stock v40306, w^{1118} ; $P\{GD10414\}v40306$;). Phenotypes produced by both *UAS-Dis3^{RNAi}* lines are indistinguishable from each other when driven by all drivers except for *69B-GAL4*, where lethality occurs at a slightly later stage (L3) for v108013. Images of adult flies were obtained by freezing the flies at -20°C for 15 minutes and then capturing a series of images at different focal depths using a Nikon D5200 camera mounted on a Nikon SMZ800 dissecting microscope. The series of images were stacked and merged in Adobe Photoshop CS6 producing the final image. For the measurement of developmental delay, crosses were set up at 25°C with flies left for 8 hours to lay eggs (8hr egg lay) with time 0 starting after the 8 hours. Times were recorded when progeny reached wandering L3, pupal and adult stages of development.

Measurement wing imaginal disc sizes

Wing imaginal discs were dissected from late L3 larvae in PBS. Late L3 larvae were staged by the addition of 0.05% bromophenol blue to the food and selecting only larvae that had cleared the dyed food from their gut. Dissected discs were mounted on poly-l-lysine slides in 85% glycerol. Disc area was measured using Axiovision 4.7 on an Axioplan microscope (Carl Zeiss).

Western blotting

Western blotting was performed on samples containing 60 wing imaginal discs. Tubulin was used as a loading control. Mouse anti-Tubulin primary antibody (Sigma, cat. no. T9026) was used at a 1:2,000

dilution with an anti-mouse-HRP conjugated secondary antibody (Sigma, cat. no. A2304) at 1:80,000. Rabbit anti-Dis3⁷ was used at 1:1,500 with an anti-rabbit-HRP conjugated secondary antibody (Sigma, cat. no. 1949) at 1:80,000. Antibody binding was detected using Amersham ECL detection reagents (GE Healthcare, cat. no. RPN2209). Relative quantification of bands was performed with ImageJ software.

Immunocytochemistry

Immunocytochemistry was performed essentially as described in ⁴⁵. Images were taken with a Zeiss Axiovert confocal microscope equipped with a LSM520 Meta. Anti-Cleaved Caspase-3 (Asp175) (Cell Signalling, cat no. 9661) was used at 1:400 dilution. Cy3-conjugated monoclonal donkey anti-mouse IgG secondary antibody was used at 1:400 (Jackson ImmunoResearch, cat. no.715-165-151).

RNA extraction and qRT-PCR

RNA extractions were performed using a miRNeasy RNA extraction kit (Qiagen, cat. no. 217084), with an on-column DNase digestion (Qiagen, cat. no. 79254). RNA concentrations were measured on a NanoDrop 1000 spectrophotometer (Thermo Scientific). For qRT-PCR, RNA samples were diluted to a consistent concentration then cDNA was prepared in duplicate using a High Capacity cDNA Reverse Transcription Kit (Life Technologies, cat. no. 4368814) with random primers. A control "no RT" reaction was performed in parallel to confirm that all genomic DNA had been degraded. qRT-PCR was performed on each cDNA replicate in duplicate (i.e. four technical replicates in total), using TaqMan Universal PCR Master Mix, No AmpErase UNG (Life Technologies, cat. no. 4324018) and an appropriate custom designed TaqMan pre-miRNA assay (Life Technologies). For custom pre-miRNA assays, the pre-miRNA hairpin sequence (miRBase) was submitted to Life Technologies' web-based Custom TaqMan Assay Design Tool as in ⁵ (**Supplemental Fig. 4**). *RpL32* (*Rp49*) was used for normalisation. For miRNA qRT-PCR, RNA was diluted to 2ng/μl then cDNA was prepared in duplicate from 10ng RNA using a TaqMan miRNA Reverse Transcription Kit (Life Technologies, cat. no. 4366596) with miRNA specific primers. As above a no RT reaction was performed in parallel. qRT-PCR was performed as above. *snoR442* was used for normalisation.

Small RNA sequencing

RNA extraction was performed as above from 60 wandering L3 wing imaginal discs. RNA integrity was checked using an Agilent 2100 Bioanalyser. 1µg total RNA was sent to ARK genomics for sample preparation and sequencing. Libraries were prepared using an Illumina TruSeq small RNA kit and size selected to specifically contain RNAs of 18-22bp in length. Samples were run across 2 lanes of a GA2 sequencer to give between 12 and 22 million reads per sample. Analysis was completed by ARK Genomics. Adaptors were removed using Cutadapt.⁴⁶ The remaining reads were mapped to miRBase release19 using Bowtie 2.⁴⁷ Mapped reads were normalised per million reads (RPKM). The total number of reads per sample ranged between 12 and 22 million, of which on average 1.12% mapped to mature miRNAs. This low percentage of miRNA mapped reads was due to with the presence of 2S rRNA which would have been retained during the size selection. miRNAs that varied significantly between parental lines were excluded from further analysis (outliers in **Fig. 3 panel C**). In addition we also removed any miRNAs whose expression differed more than 2-fold between biological replicates of the same genotype. Finally we only selected miRNAs that changed in expression under the test conditions more than 2-fold against all parental replicates for further analysis. One miRNA was selected that did not pass these filters. *miR-987-5p* expression varied between parental controls, however due to it showing the greatest level of upregulation following Dis3 knockdown against both separate parents, it was taken for further analysis. Due to the overall similarity between the two parental controls (**Fig. 3 panel C**) we were able to group them together into an overall 'control' group. All comparisons shown are between the Dis3 knockdown samples and the grouped parental controls.

Identification of known and novel miRNAs

Fastq files were converted to fasta files using the FASTX toolkit (http://hannonlab.cshl.edu/fastx_toolkit/). Reads were simultaneously clipped and mapped using the mapper.pl script included in miRDeep2.³⁴ Reads were mapped to the *Drosophila melanogaster* genome, version BDGP5 (Ensembl) (Settings:-c -j -k -l 17 -m). To identify novel miRNAs miRDeep2.pl was used. *Drosophila simulans*, *Drosophila sechellia*, *Drosophila erecta*, *Drosophila yakuba* and *Drosophila ananassae* were used as similar species to aid the identification of novel miRNAs. Potential novel miRNAs were selected for further analysis if they were found in at least

five of the six replicates, including at least one of each genotype. The only selected potential novel miRNA was validated using custom TaqMan assays to the identified sequence (CACAU CGAUGUUUUUCCACCUC). qRT-PCR was completed with the custom assay as above. The secondary structure of the novel miRNA was predicted using RNAfold WebServer (<http://rna.tbi.univie.ac.at/cgi-bin/RNAfold.cgi>) with default settings.

Statistical analyses

All statistical analyses were performed in GraphPad Prism 6 except for density and scatter plots which were produced in R (version 3.1.1). All data analysed were compatible with parametric tests. Two-sided two-sample t-tests were used to compare the means of single test groups to single control groups. If multiple comparisons were required, a one-way ANOVA was performed with a post-test to compare the means of each possible pair of samples.

Acknowledgements

The authors would like to thank Clare Rizzo-Singh and Karen Scruby for technical help and Julie Aspden for helpful discussions. This work was funded by a Brighton and Sussex Medical School studentship, the Biotechnology and Biological Sciences Research Council [grant numbers BB/I021345/1 and BB/G002754/1], a Medical Research Council Studentship and Medical Research Council Centenary Award [G1000409, MR/J500525/1], FCT-Portugal [grant numbers EXPL/BEX-BCM/1317/2013 and Pest-OE/EQB/LA0004/2013], and the European Commission [grant number FP7- KBBE-2013-1-289326].

References

1. Jones CI, Zabolotskaya MV, Newbury SF. The 5' → 3' exoribonuclease XRN1/Pacman and its functions in cellular processes and development. *Wiley Interdiscip Rev RNA* 2012;3:455-68.
2. Arraiano CM, Mauxion F, Viegas SC, Matos RG, Seraphin B. Intracellular ribonucleases involved in transcript processing and decay: precision tools for RNA. *Biochim Biophys Acta* 2013;1829:491-513.
3. Reis FP, Pobre V, Silva IJ, Malecki M, Arraiano CM. The RNase II/RNB family of exoribonucleases: putting the 'Dis' in disease. *Wiley Interdiscip Rev RNA* 2013;4:607-15.

4. Jones CI, Newbury SF. Functions of microRNAs in *Drosophila* development. *Biochem Soc Trans* 2010;38:1137-43.
5. Jones CI, Grima DP, Waldron JA, Jones S, Parker HN, Newbury SF. The 5'-3' exoribonuclease Pacman (Xrn1) regulates expression of the heat shock protein Hsp67Bc and the microRNA miR-277-3p in *Drosophila* wing imaginal discs. *RNA Biol* 2013;10:1345-55.
6. Waldron JA, Jones CI, Towler BP, Pashler AL, Grima DP, Hebbes DP, et al. Xrn/Pacman affects apoptosis and regulates expression of *hid* and *reaper*. *Biology Open* 2015; doi: 10.1242/bio.201410199.
7. Cairrao F, Arraiano C, Newbury S. *Drosophila* gene *tazman*, an orthologue of the yeast exosome component Rrp44p/Dis3, is differentially expressed during development. *Dev Dyn* 2005;232:733-7.
8. Malecki M, Viegas SC, Carneiro T, Golik P, Dressaire C, Ferreira MG, et al. The exoribonuclease Dis3L2 defines a novel eukaryotic RNA degradation pathway. *EMBO J* 2013;32:1842-54.
9. Mitchell P, Petfalski E, Shevchenko A, Mann M, Tollervey D. The exosome: a conserved eukaryotic RNA processing complex containing multiple 3'-5' exoribonucleases. *Cell* 1997;91:457-66.
10. Halbach F, Reichelt P, Rode M, Conti E. The yeast ski complex: crystal structure and RNA channeling to the exosome complex. *Cell* 2013;154:814-26.
11. Tomecki R, Kristiansen MS, Lykke-Andersen S, Chlebowski A, Larsen KM, Szczesny RJ, et al. The human core exosome interacts with differentially localized processive RNases: hDIS3 and hDIS3L. *EMBO J* 2010;29:2342-57.
12. Staals RH, Bronkhorst AW, Schilders G, Slomovic S, Schuster G, Heck AJ, et al. Dis3-like 1: a novel exoribonuclease associated with the human exosome. *EMBO J* 2010;29:2358-67.
13. Schneider C, Leung E, Brown J, Tollervey D. The N-terminal PIN domain of the exosome subunit Rrp44 harbors endonuclease activity and tethers Rrp44 to the yeast core exosome. *Nucleic Acids Res* 2009;37:1127-40.
14. Schaeffer D, Reis FP, Johnson SJ, Arraiano CM, van Hoof A. The CR3 motif of Rrp44p is important for interaction with the core exosome and exosome function. *Nucleic Acids Res* 2012;40:9298-307.

15. Schaeffer D, Tsanova B, Barbas A, Reis FP, Dastidar EG, Sanchez-Rotunno M, et al. The exosome contains domains with specific endoribonuclease, exoribonuclease and cytoplasmic mRNA decay activities. *Nat Struct Mol Biol* 2009;16:56-62.
16. Chang HM, Triboulet R, Thornton JE, Gregory RI. A role for the Perlman syndrome exonuclease Dis3L2 in the Lin28-let-7 pathway. *Nature* 2013;497:244-8.
17. Lubas M, Damgaard CK, Tomecki R, Cysewski D, Jensen TH, Dziembowski A. Exonuclease hDIS3L2 specifies an exosome-independent 3'-5' degradation pathway of human cytoplasmic mRNA. *EMBO J* 2013;32:1855-68.
18. Ustianenko D, Hrossova D, Potesil D, Chalupnikova K, Hrazdilova K, Pachernik J, et al. Mammalian DIS3L2 exoribonuclease targets the uridylated precursors of let-7 miRNAs. *RNA* 2013;19:1632-8.
19. Graham AC, Davis SM, Andrulis ED. Interdependent nucleocytoplasmic trafficking and interactions of Dis3 with Rrp6, the core exosome and importin-alpha3. *Traffic* 2009;10:499-513.
20. Mamolen M, Smith A, Andrulis ED. Drosophila melanogaster Dis3 N-terminal domains are required for ribonuclease activities, nuclear localization and exosome interactions. *Nucleic Acids Res* 2010;38:5507-17.
21. Chlebowski A, Lubas M, Jensen TH, Dziembowski A. RNA decay machines: the exosome. *Biochim Biophys Acta* 2013;1829:552-60.
22. Gudipati RK, Xu Z, Lebreton A, Seraphin B, Steinmetz LM, Jacquier A, et al. Extensive degradation of RNA precursors by the exosome in wild-type cells. *Mol Cell* 2012;48:409-21.
23. Sloan KE, Schneider C, Watkins NJ. Comparison of the yeast and human nuclear exosome complexes. *Biochem Soc Trans* 2012;40:850-5.
24. Tomecki R, Drazkowska K, Kucinski I, Stodus K, Szczesny RJ, Gruchota J, et al. Multiple myeloma-associated hDIS3 mutations cause perturbations in cellular RNA metabolism and suggest hDIS3 PIN domain as a potential drug target. *Nucleic Acids Res* 2014;42:1270-90.
25. Chapman MA, Lawrence MS, Keats JJ, Cibulskis K, Sougnez C, Schinzel AC, et al. Initial genome sequencing and analysis of multiple myeloma. *Nature* 2011;471:467-72.
26. Ding L, Ley TJ, Larson DE, Miller CA, Koboldt DC, Welch JS, et al. Clonal evolution in relapsed acute myeloid leukaemia revealed by whole-genome sequencing. *Nature* 2012;481:506-10.

27. Parsons DW, Li M, Zhang X, Jones S, Leary RJ, Lin JC, et al. The genetic landscape of the childhood cancer medulloblastoma. *Science* 2011;331:435-9.
28. Rose AE, Poliseno L, Wang J, Clark M, Pearlman A, Wang G, et al. Integrative genomics identifies molecular alterations that challenge the linear model of melanoma progression. *Cancer Res* 2011;71:2561-71.
29. Liu X, Zheng Q, Vrettos N, Maragkakis M, Alexiou P, Gregory BD, et al. A MicroRNA precursor surveillance system in quality control of MicroRNA synthesis. *Mol Cell* 2014;55:868-79.
30. Flynt AS, Greimann JC, Chung WJ, Lima CD, Lai EC. MicroRNA biogenesis via splicing and exosome-mediated trimming in *Drosophila*. *Mol cell* 2010;38:900-7.
31. Hou D, Ruiz M, Andrulis ED. The ribonuclease Dis3 is an essential regulator of the developmental transcriptome. *BMC Genomics* 2012;13:359.
32. Kiss DL, Andrulis ED. Genome-wide analysis reveals distinct substrate specificities of Rrp6, Dis3, and core exosome subunits. *RNA* 2010;16:781-91.
33. Flybase. The *Drosophila* genetic database. *Nucleic Acids Res* 1996;24:53-6.
34. Friedlander MR, Chen W, Adamidi C, Maaskola J, Einspanier R, Knespel S, et al. Discovering microRNAs from deep sequencing data using miRDeep. *Nat Biotechnol* 2008;26:407-15.
35. Graham AC, Kiss DL, Andrulis ED. Differential distribution of exosome subunits at the nuclear lamina and in cytoplasmic foci. *Mol Biol Cell* 2006;17:1399-409.
36. Bejarano F, Bortolamiol-Becet D, Dai Q, Sun K, Saj A, Chou YT, et al. A genome-wide transgenic resource for conditional expression of *Drosophila* microRNAs. *Development* 2012;139:2821-31.
37. Schertel C, Rutishauser T, Forstemann K, Basler K. Functional characterization of *Drosophila* microRNAs by a novel in vivo library. *Genetics* 2012;192:1543-52.
38. Lee M, Choi Y, Kim K, Jin H, Lim J, Nguyen TA, et al. Adenylation of maternally inherited microRNAs by Wispy. *Mol cell* 2014;56:696-707.
39. Han BW, Hung JH, Weng Z, Zamore PD, Ameres SL. The 3'-to-5' exoribonuclease Nibbler shapes the 3' ends of microRNAs bound to *Drosophila* Argonaute1. *Curr Biol* 2011;21:1878-87.
40. Chatterjee S, Grosshans H. Active turnover modulates mature microRNA activity in *Caenorhabditis elegans*. *Nature* 2009;461:546-9.

41. Fatica A, Bozzoni I. Long non-coding RNAs: new players in cell differentiation and development. *Nat Rev Genet* 2014;15:7-21.
42. Forstemann K, Tomari Y, Du T, Vagin VV, Denli AM, Bratu DP, et al. Normal microRNA maturation and germ-line stem cell maintenance requires Loquacious, a double-stranded RNA-binding domain protein. *PLoS Biol* 2005;3:e236.
43. Michlewski G, Guil S, Caceres JF. Stimulation of pri-miR-18a processing by hnRNP A1. *Adv Exp Med Biol* 2010;700:28-35.
44. Liu N, Abe M, Sabin LR, Hendriks GJ, Naqvi AS, Yu Z, et al. The exoribonuclease Nibbler controls 3' end processing of microRNAs in *Drosophila*. *Curr Biol* 2011;21:1888-93.
45. Sullivan W, Ashburner A, Hawley RS. *Drosophila* Protocols. New York, USA: Cold Spring Harbor Laboratory Press, 2000.
46. Chen C, Khaleel SS, Huang H, Wu CH. Software for pre-processing Illumina next-generation sequencing short read sequences. *Source code for biology and medicine* 2014;9:8.
47. Langmead B, Salzberg SL. Fast gapped-read alignment with Bowtie 2. *Nat Methods* 2012;9:357-9.
48. Stark A, Brennecke J, Russell RB, Cohen SM. Identification of *Drosophila* MicroRNA targets. *PLoS Biol* 2003;1:E60.
49. Esslinger SM, Schwalb B, Helfer S, Michalik KM, Witte H, Maier KC, et al. *Drosophila* miR-277 controls branched-chain amino acid catabolism and affects lifespan. *RNA Biol* 2013;10:1042-56.
50. Marrone AK, Edeleva EV, Kucherenko MM, Hsiao NH, Shcherbata HR. Dg-Dys-Syn1 signaling in *Drosophila* regulates the microRNA profile. *BMC Cell Biol* 2012;13:26.
51. Vlachos IS, Paraskevopoulou MD, Karagkouni D, Georgakilas G, Vergoulis T, Kanellos I, et al. DIANA-TarBase v7.0: indexing more than half a million experimentally supported miRNA:mRNA interactions. *Nucleic Acids Res* 2015;43:D153-9.
52. Liu N, Landreh M, Cao K, Abe M, Hendriks GJ, Kennerdell JR, et al. The microRNA miR-34 modulates ageing and neurodegeneration in *Drosophila*. *Nature* 2012;482:519-23.
53. Yamamoto A, Zwarts L, Callaerts P, Norga K, Mackay TF, Anholt RR. Neurogenetic networks for startle-induced locomotion in *Drosophila melanogaster*. *Proc Natl Acad Sci U S A* 2008;105:12393-8.

Figure Legends

Figure 1: Knockdown of Dis3 in the wing imaginal disc results in severe developmental phenotypes. Knockdown of Dis3 in the wing pouch of the wing imaginal disc results in a "no wing" phenotype at 100% penetrance (*Dis3^{KD}*) (B) when compared to a *UAS-Dis3^{RNAi}* parental control male fly (*Dis3^{WT}*) (A). (C') Knockdown of Dis3 protein in *nub-GAL4/+ ; UAS-Dis3^{RNAi}/+* wing imaginal discs by Western blotting. *Dis3^{WT}* genotype: ; *nub-Gal4* ;. (C'') Dis3 expression is knocked down to 20% of parental controls in wing imaginal discs when *UAS-Dis3^{RNAi}* is driven by *nub-GAL4*. '*Dis3^{WT}*' includes parental genotypes ; *nub-Gal4* ; and ; *UAS-Dis3^{RNAi}*. $n \geq 3$, $p = 0.0009$, error bars show standard error. (D and E) *nub-GAL4/+ ; UAS-Dis3^{RNAi}/+* flies also show a severe lack of haltere development (E) (100% penetrance) compared to parental control flies (D). (F) Dis3 knockdown progeny (*nub-GAL4/+ ; UAS-Dis3^{RNAi}/+*) are delayed in larval development by 40 hours (red) when compared to parental controls (black – *UAS-Dis3^{RNAi}* and *nub-GAL4*) ($n \geq 23$).

Figure 2: Dis3 knockdown in the wing pouch of the wing imaginal discs results in small wing discs and extensive apoptosis. (A and B) Dis3 knockdown (*nub-GAL4/+ ; UAS-Dis3^{RNAi}/+*) late L3 wing imaginal discs (B) are smaller than parental control (*Dis3^{WT}* is ; *UAS-Dis3^{RNAi}*) wing imaginal discs (A) (scale bar=50µm). (C) Quantitation of *nub-GAL4* driven Dis3 knockdown wing imaginal discs shows that they are 23% smaller than parental control discs ('*Dis3^{WT}*' includes parental genotypes ; *nub-GAL4* ; and ; *UAS-Dis3^{RNAi}*). ($n \geq 21$, $p < 0.0001$, error bars represent standard error). (D and E) Knockdown of Dis3 in the wing pouch results in apoptosis specifically localised within the wing pouch region (E) while parental control discs show very little apoptotic activity (D). ($n \geq 26$, scale bar=50µm).

Figure 3: Expression patterns of miRNA in wing imaginal discs. (A) Kernel density plot of the general distribution of the 109 detected miRNAs indicates 2 peaks of miRNA expression. Knockdown of Dis3 results in a shift in the poorly expressed miRNAs (left hand peak) to a higher level of expression compared to the more highly expressed miRNAs which do not change (right hand peak). (B) Distribution of fold changes between both parents (Control) and grouped parents vs Dis3 knockdown (*Dis3^{KD}*). Knockdown of Dis3 results in the emergence of peaks around +/- 2-fold change. Dotted vertical lines represent +/- 2-fold change. (C) Comparison of miRNA RPKMs between the two parental controls shows high similarity. Dotted lines show +/- 2-fold change. (D) Comparison of

miRNA RPKM between grouped parental controls (Control) and Dis3 knockdown (*Dis3^{KD}*) wing imaginal discs. Blue and red dotted lines represent +2-fold change and -2-fold change respectively. Selected miRNAs that increase or decrease in expression following Dis3 knockdown are coloured in blue and red respectively. Selected miRNAs that remain unchanged are highlighted in green. (E) 61.5% of miRNAs in the wing imaginal disc do not change in expression following the knockdown of Dis3. 26.6% of miRNAs increase in expression ≥ 1.5 -fold (10.1% ≥ 2 -fold). 11.9% of miRNAs decrease in expression ≥ 1.5 -fold (5.5% ≥ 2 -fold).

Figure 4: Effect of Dis3 knockdown on all wing imaginal disc miRNAs detected above threshold levels. Fold changes (*Dis3^{KD}* vs grouped parental controls) from miRNA-seq data of the 109 detected miRNAs in the wing imaginal disc. *miR-987-5p* shows the greatest increase in expression (49.5-fold) whilst *miR-125-5p* shows the greatest decrease in expression (-2.4-fold). miRNAs that increase ≥ 2 -fold are highlighted in blue font and those selected for further analysis are shown with blue bars. miRNAs that decrease ≥ 2 -fold are highlighted in red font and those selected for further analysis shown with red bars. Selected miRNAs that remain unchanged are highlighted in green font. Dotted lines represent +/-2-fold changes. ($n \geq 2$, error bars represent standard error).

Figure 5: Identification of a novel mature miRNAs in the wing imaginal disc. Using miRDeep2 we identified a novel miRNA of moderate expression in the wing imaginal discs. The predicted pre-miRNA forms a hairpin loop secondary structure with the novel miRNA being situated at the 3' end (shown in pink). The novel miRNA was detected at moderate levels using miRNA-seq in all but one sample. Validation of the miRNA using qRT-PCR shows that this novel miRNA is expressed at similar levels to *miR-277-3p* in all samples.

Figure 6: qRT-PCR validation of misexpressed miRNAs from the miRNA sequencing data. (A) Grouping of RPKM of selected miRNAs for all replicates is highly consistent between controls (black dots) and knockdown replicates (red dots). (B) Validation of miRNA-seq fold changes (red dots) using qRT-PCR. All selected miRNAs that change in expression upon Dis3-depletion in the miRNA-seq data also significantly change in expression when using qRT-PCR (except *miR-7-3p*). Dotted lines show +/-2-fold changes. Stars represent levels of significance calculated using a two sample t-test.

(**** $p < 0.0001$, ** $p < 0.01$, * $p < 0.05$ $n \geq 3$, error bars represent standard error). (C) The pri/pre-miRNA levels were measured for the miRNAs that significantly changes in expression in both the miRNA-seq and qRT-PCR data. The expression levels of *miR-252-5p* and *miR-982-5p* change post-transcriptionally following Dis3 knockdown. All other miRNAs alter in a transcriptional manner as the pri/pre-mRNA (light grey) also changes significantly in expression, similar to the levels observed mature miRNAs (dark grey). Dotted lines show +/-2-fold changes. Stars represent levels of significance calculated using a two sample t-test. **** $p < 0.0001$, ** $p < 0.01$, * $p < 0.05$, ns $p > 0.05$. ($n \geq 3$, error bars represent standard error).

Figure 7: Overexpression of *miR-252* in the wing pouch of the imaginal disc results in severe wing phenotypes. (A) Overexpression of *miR-252* using the ubiquitously expressed *tub-GAL4* driver results in 100% lethality compared to controls (*UAS-miR-252/TM6*). $n=184$. (B) Overexpression of *UAS-miR-252* in the wing pouch using the *nubbin-GAL4* driver results in a 1056-fold increase in *miR-252-5p* expression in the wing imaginal disc. ($n \geq 3$, $p < 0.0001$, error bars represent standard error). (C and D) Overexpression of *UAS-miR-252* in the wing pouch of the wing imaginal disc using the *nubbin-GAL4* driver (*;nub-Gal4/+ ;UAS-miR-252/+*) results in severe wing crumpling (D) compared to a parental control (*miR-252^{WT}* is *UAS-miR-252*) (C) with 100% penetrance. $n=168$.

Figure 8: Knockdown of the exosome subunit Rrp40 results in similar phenotypes as to Dis3 knockdown. Knockdown of the exosome subunit Rrp40 using the *nubbin-GAL4* wing pouch driver (*;nub-Gal4/UAS-Rrp40^{RNAi};*) results in severe wing development phenotypes (B' and B'') when compared to parental controls (A). 90% of adults present a severe phenotype with crumpled wings (B') and the remaining 10% show a similar phenotype to Dis3 knockdown with no wings (B''). (C) Knockdown of Rrp40 in the wing pouch (*nub-GAL4*) results in a similar increase in *miR-252-5p* expression as observed during Dis3 depletion, indicating the effect observed upon Dis3 knockdown is a result of Dis3/exosome impairment ($n \geq 3$, ** $p < 0.01$, error bars represent standard error).

Supplemental Figure 1: Dis3 is also required for the correct development of the thoracic region of the wing imaginal disc. (A and B) Knockdown of Dis3 driven by *pnr-GAL4* (*;UAS-Dis3^{RNAi}/pnr-GAL4*) results in a 100% penetrant severe cleft thorax phenotype (*Dis3^{KD}*)(B) when compared to the

thoracic region of a parental control male fly (*Dis3^{WT}*) (A). (C) Knockdown by *pnr-GAL4* also results in pupal lethality. 80% of cross progeny are that of the internal control genotype (*Dis3^{WT}* is *UAS-Dis3^{RNAi}/TM3*). (n=329, error bars show standard error).

Supplemental Figure 2: Hierarchical clustering of replicates in miRNA-seq. The overall expression profiles of the two parental controls (;; *UAS-Dis3^{RNAi}* and ; *nub-GAL4* ;) are more similar to each other than they are to the *Dis3^{KD}* knockdown replicates (*Dis3^{KD}* full genotype: ; *nub-Gal4/+* ; *UAS-Dis3^{RNAi}/+*). Additionally the biological replicates within each genotype are more similar to each other than any replicate from either of the two genotypes.

Supplemental Figure 3: miRNA sequencing identifies 109 mature miRNAs in L3 wing imaginal discs. 109 miRNAs were detected in L3 wing imaginal discs by miRNA-seq and presented in descending order of abundance in control samples by normalised read counts (RPKM). *miR-9a-5p* was the most highly abundant whilst *miR-307a-3p* was the least abundant confidently detected miRNA. Those selected for further analysis are highlighted. Green = no change between conditions. Red = miRNAs that decreased following *Dis3* knockdown. Blue = miRNAs that increased ≥ 2 -fold in expression following *Dis3* knockdown.

Supplemental Figure 4: List of custom TaqMan assays designed to specific pri/pre-miRNAs.

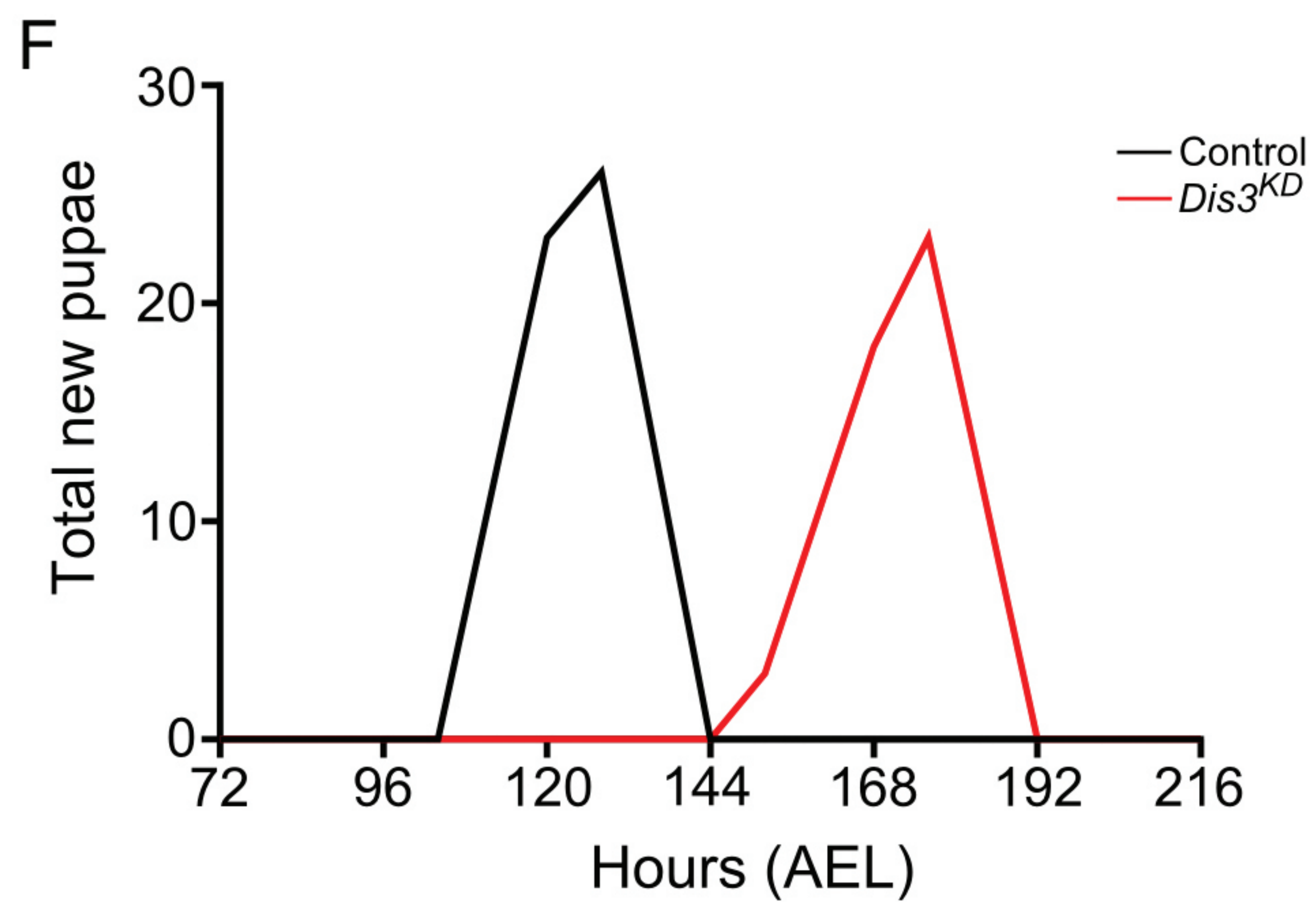
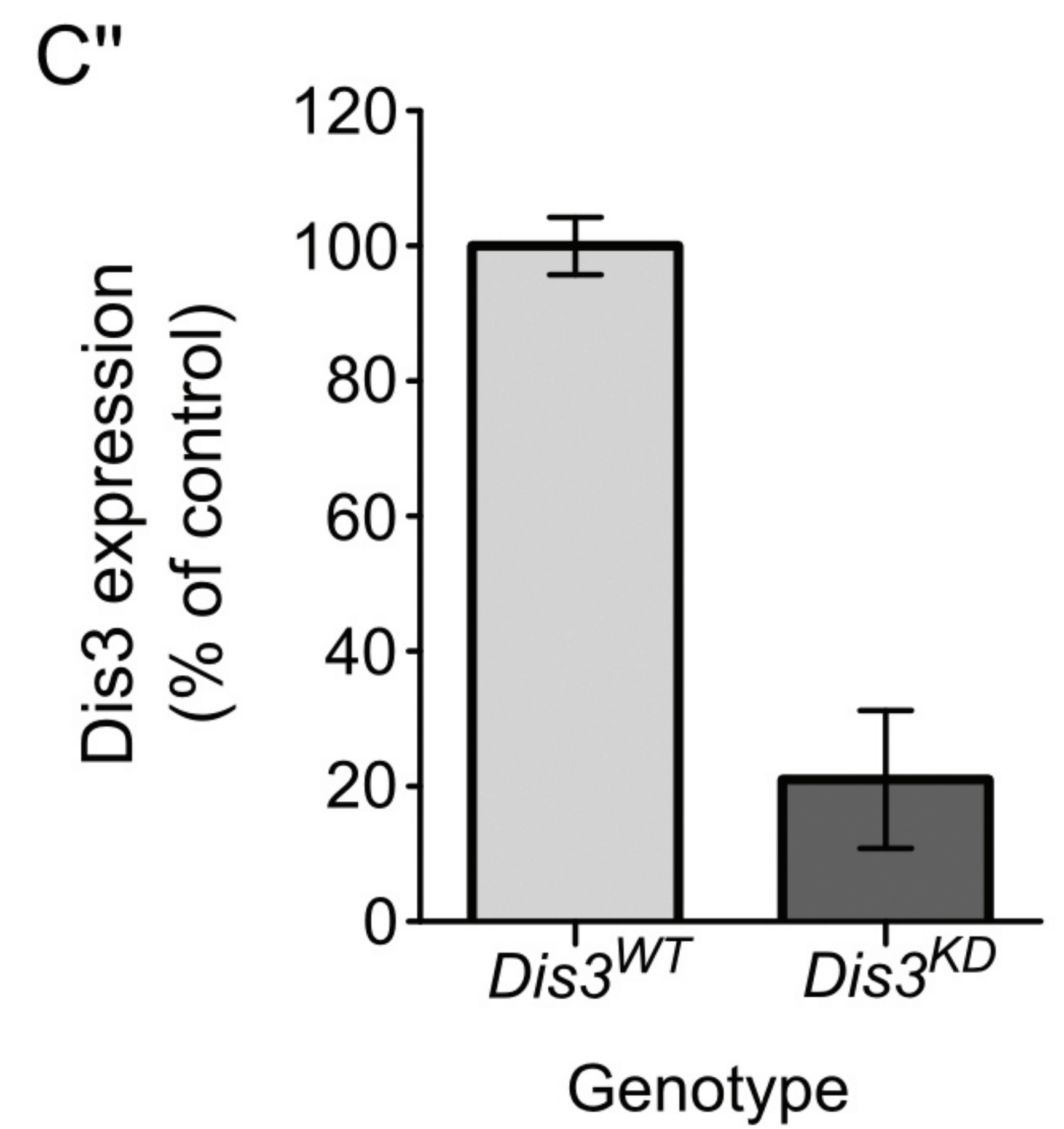
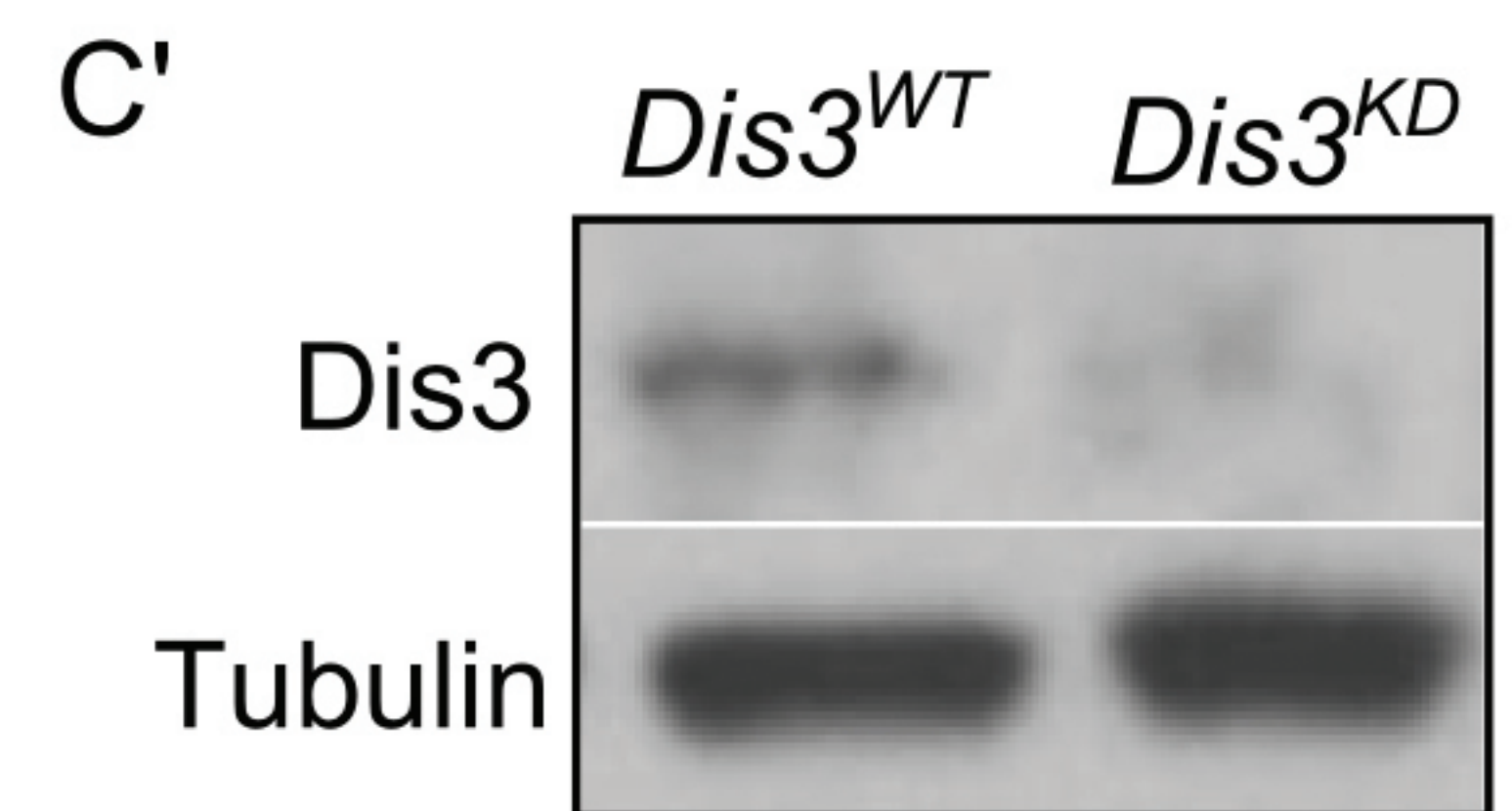
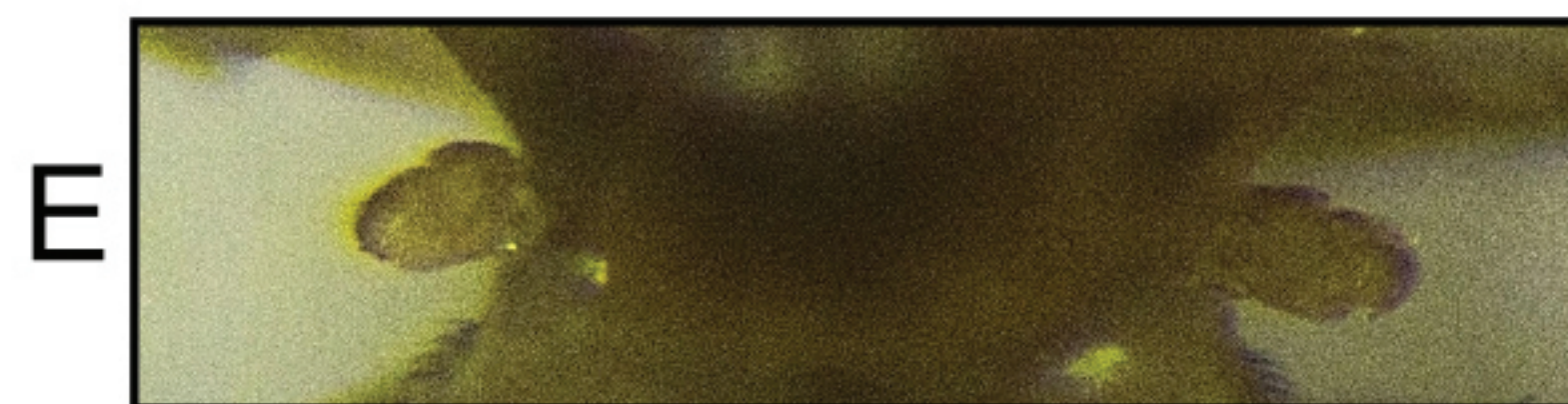
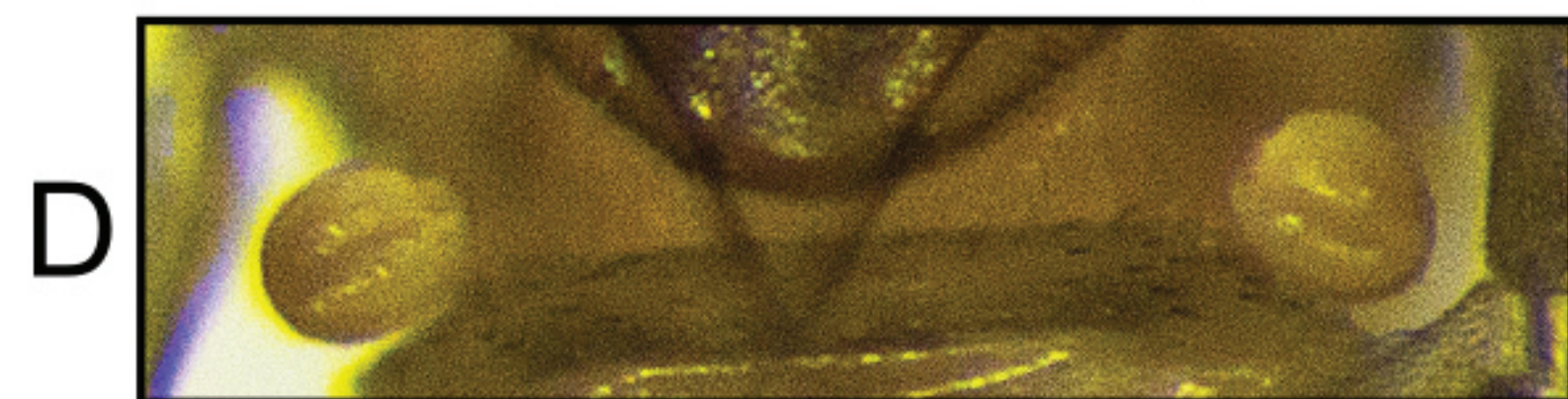
Table 1: Stages of lethality observed following ubiquitous knockdown of Dis3.

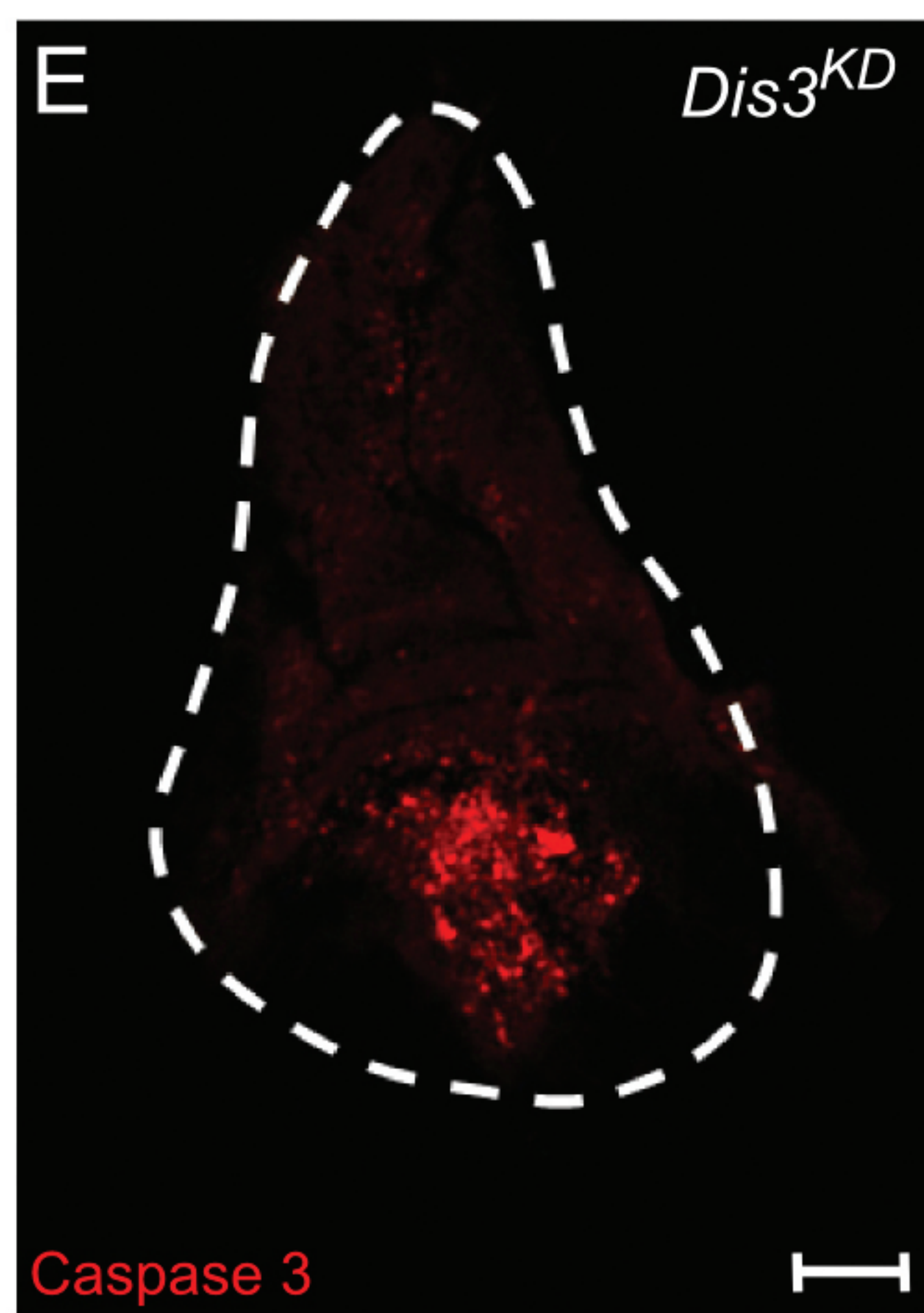
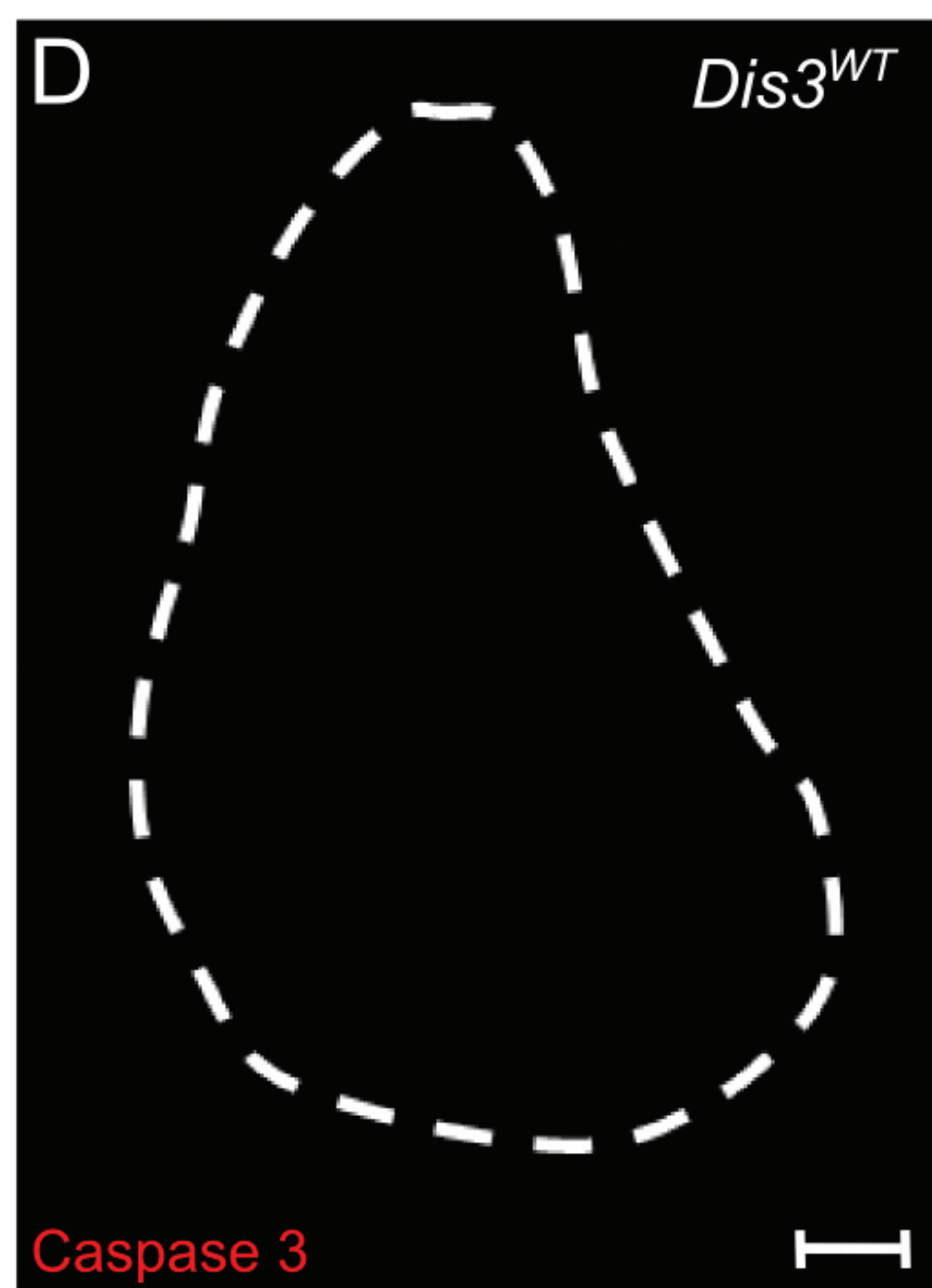
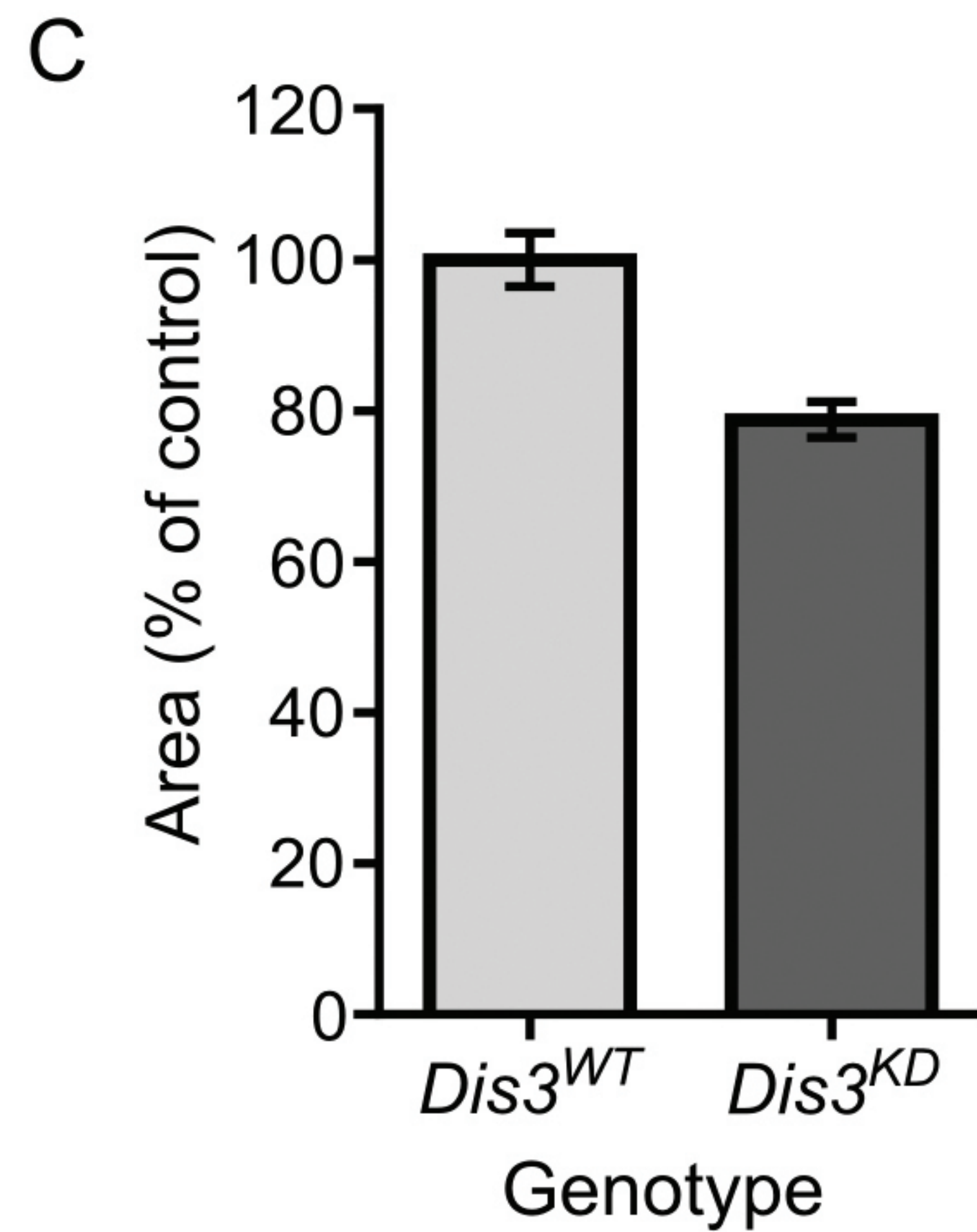
| GAL4-Driver | Region of Expression | Stage of Lethality (GD11917 v35090) | Stage of Lethality (KK101473 VIE-260B) |
|--------------------------|--|--|---|
| <i>Tubulin-GAL4</i> | Ubiquitous | L2 | L2 |
| <i>Daughterless-GAL4</i> | Ubiquitous | L2 | L2 |
| <i>69B-GAL4</i> | Ectoderm and wing, haltere, ventral thoracic and eye discs | L2 | L3 after 2 week delay |

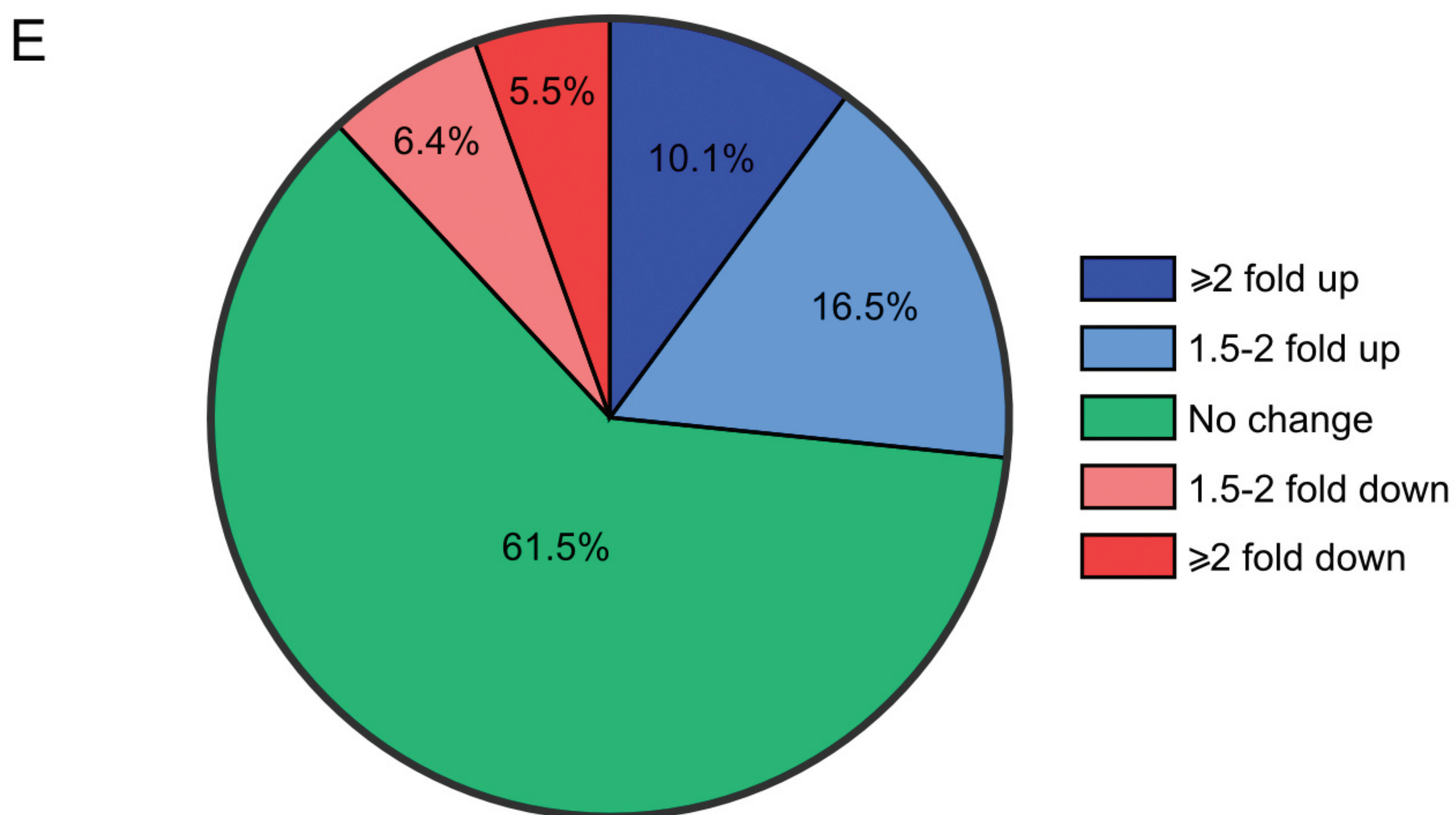
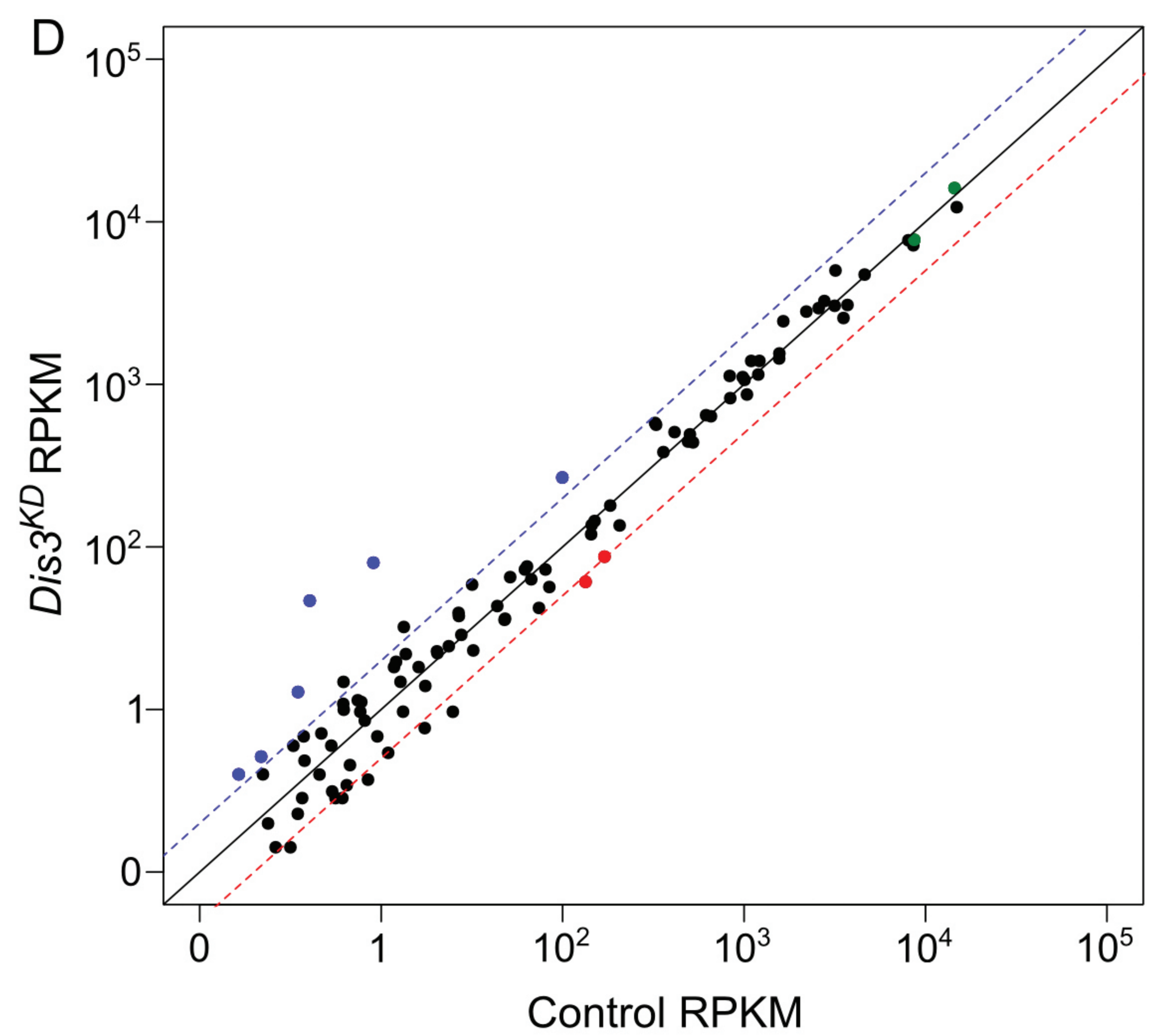
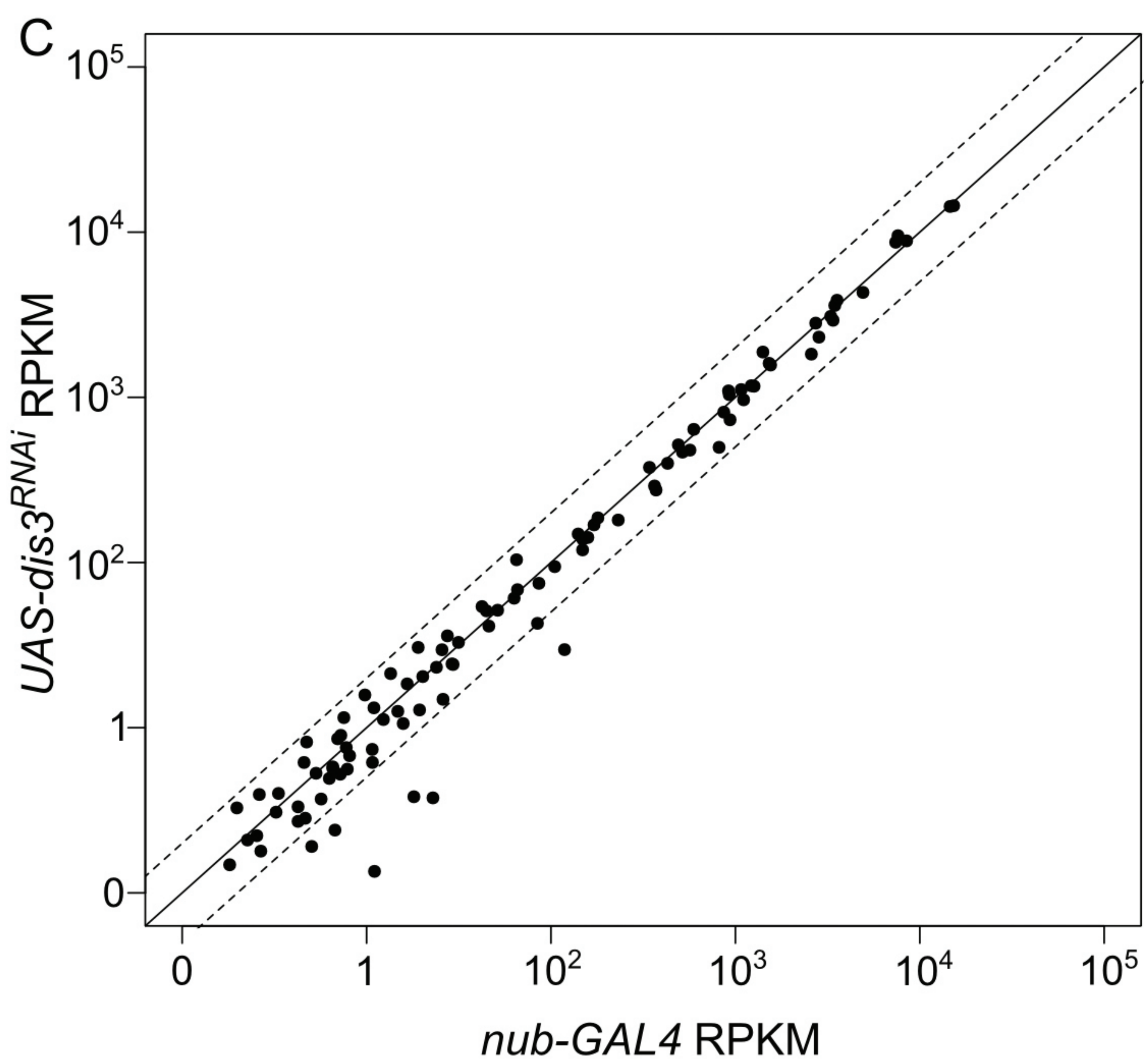
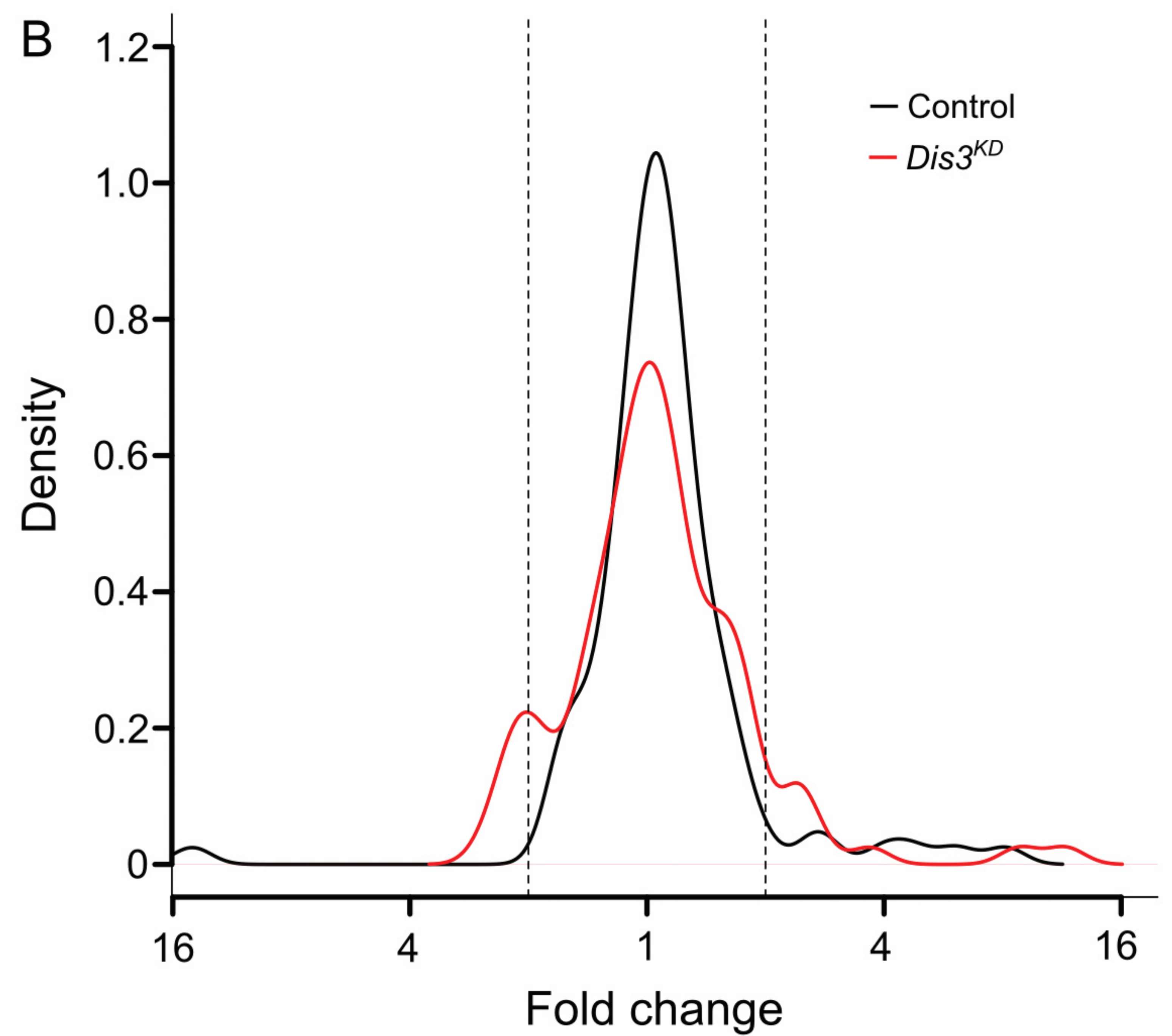
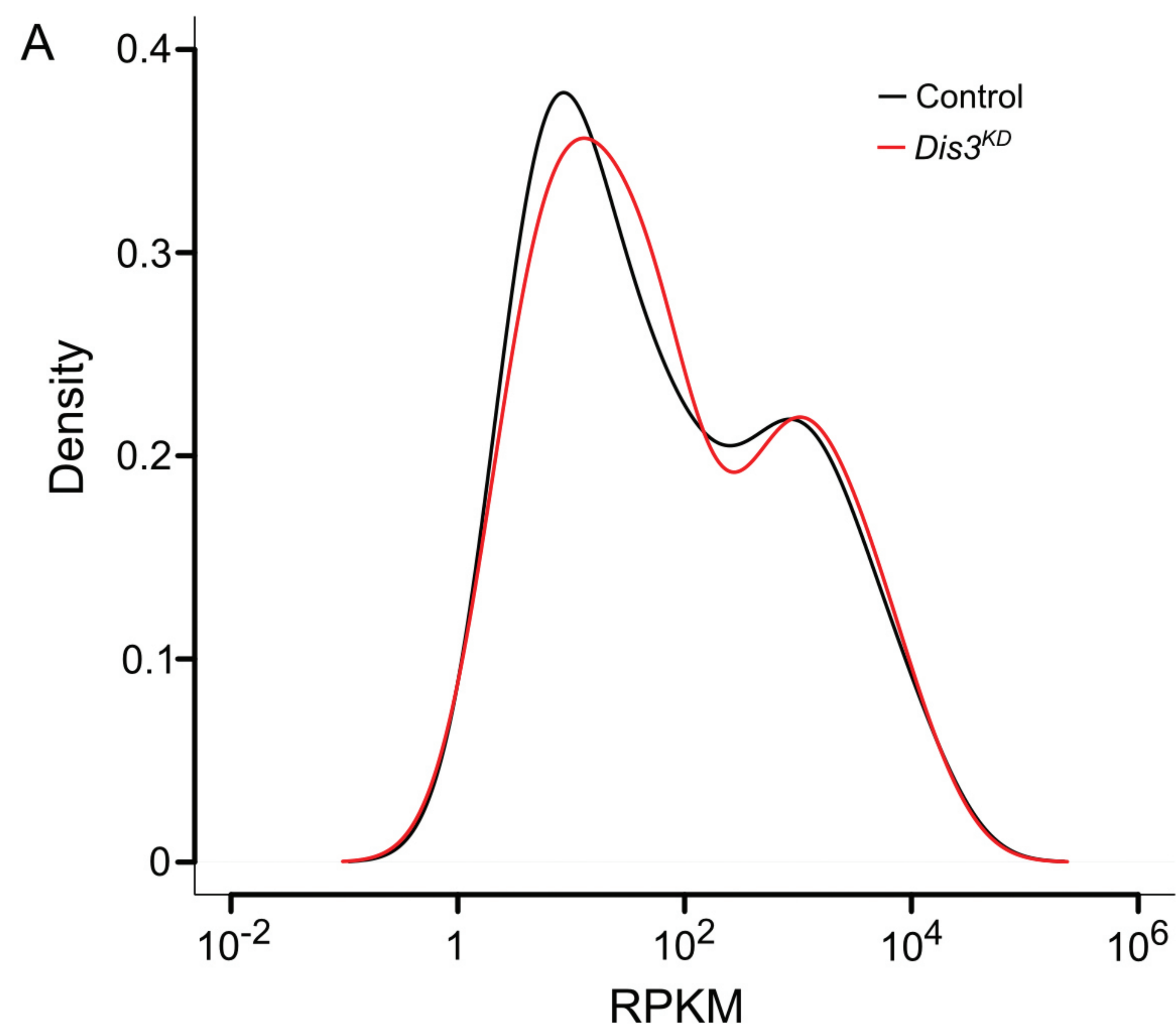
Table 2: Summary of misexpressed miRNAs in Dis3 knockdown wing imaginal discs.

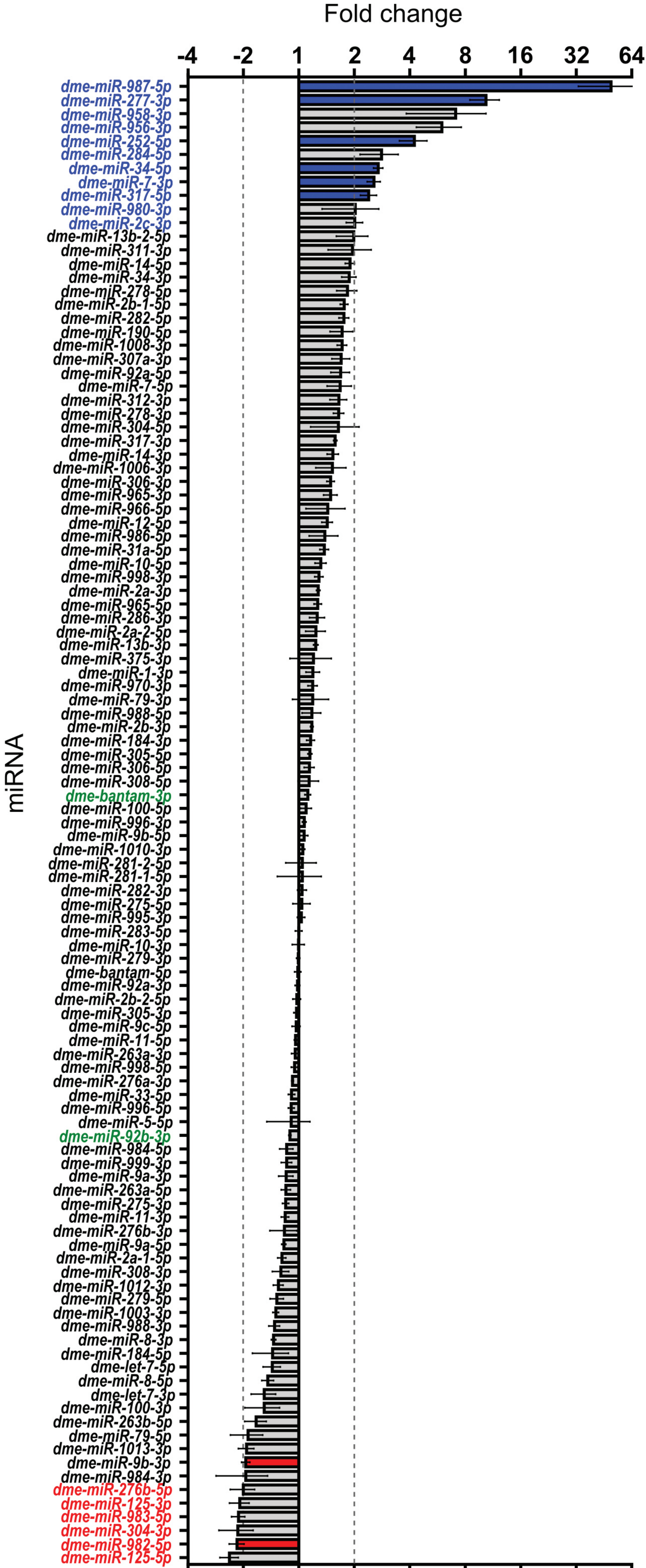
| miRNA | Fold change Seq/qRT-PCR | Conservation | Known function in <i>Drosophila</i> | Validated targets in <i>Drosophila</i> | Clustering (same transcriptional unit) | References |
|-------------------|----------------------------|--------------------|---|--|--|-------------------|
| <i>miR-987-5p</i> | +49.5/+16.8 | Dm | Unknown | None identified | No | |
| <i>miR-277-3p</i> | +10.4/+3.7 | Dm | Controls valine leucine and isoleucine degradation | None identified | <i>miR-34</i> | ^{48, 49} |
| <i>miR-252-5p</i> | +4.2/+2.1 | Sp, Dm, Ce, | Misregulated in stress and dystrophy | None identified | No | ⁵⁰ |
| <i>miR-34-5p</i> | +2.7/+1.4 | Hs, Sp, Dm, Ce | Negative regulation of neuronal cell death | <i>Su(z)12</i> , <i>Eip74EF</i> | <i>miR-277</i> | ^{51, 52} |
| <i>miR-317-5p</i> | +2.4/2.1 | D | Brain morphogenesis | None identified | No* | ⁵³ |
| <i>miR-9b-3p</i> | -2.0/-1.5 | Hs, Sp, Dm, Ce, | Unknown | None identified | <i>miR-9c</i> , <i>miR-306</i> and <i>miR-79</i> . | |
| <i>miR-982-5p</i> | -2.2/-4.4 | Dm | Unknown | None identified | No** | |

Hs – *Homo sapiens*, Sp – *Strongylocentrotus purpuratus*, Dm – *Drosophila melanogaster*, Ce – *Caenorhabditis elegans*. **miR-317* is located in close proximity to *miR-34* and *miR-277*. ***miR-982* is located in close proximity to *miR-984*, *miR-303*, *miR-983-1* and *miR-983-2*. Conservation taken from miRBase release 19.



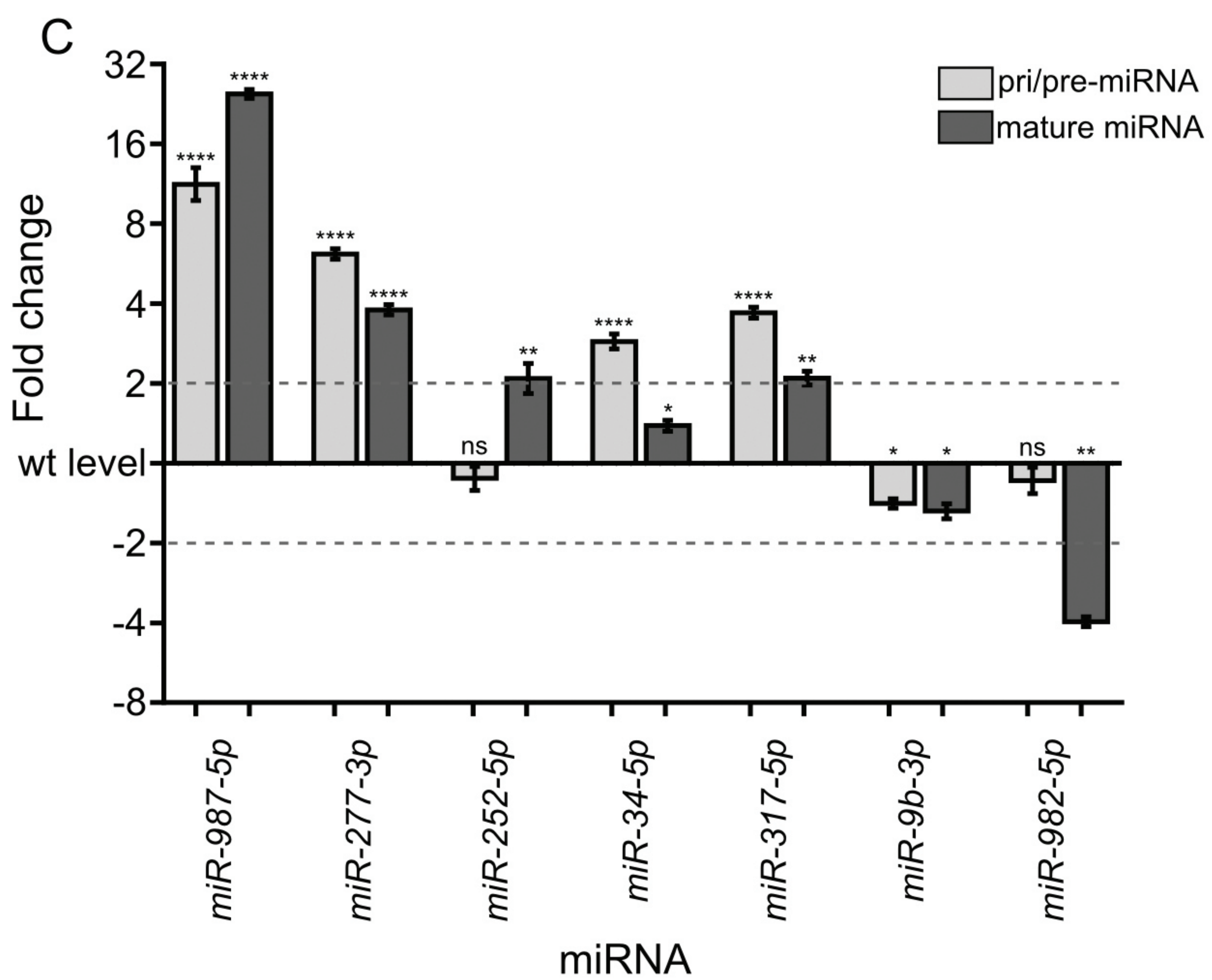
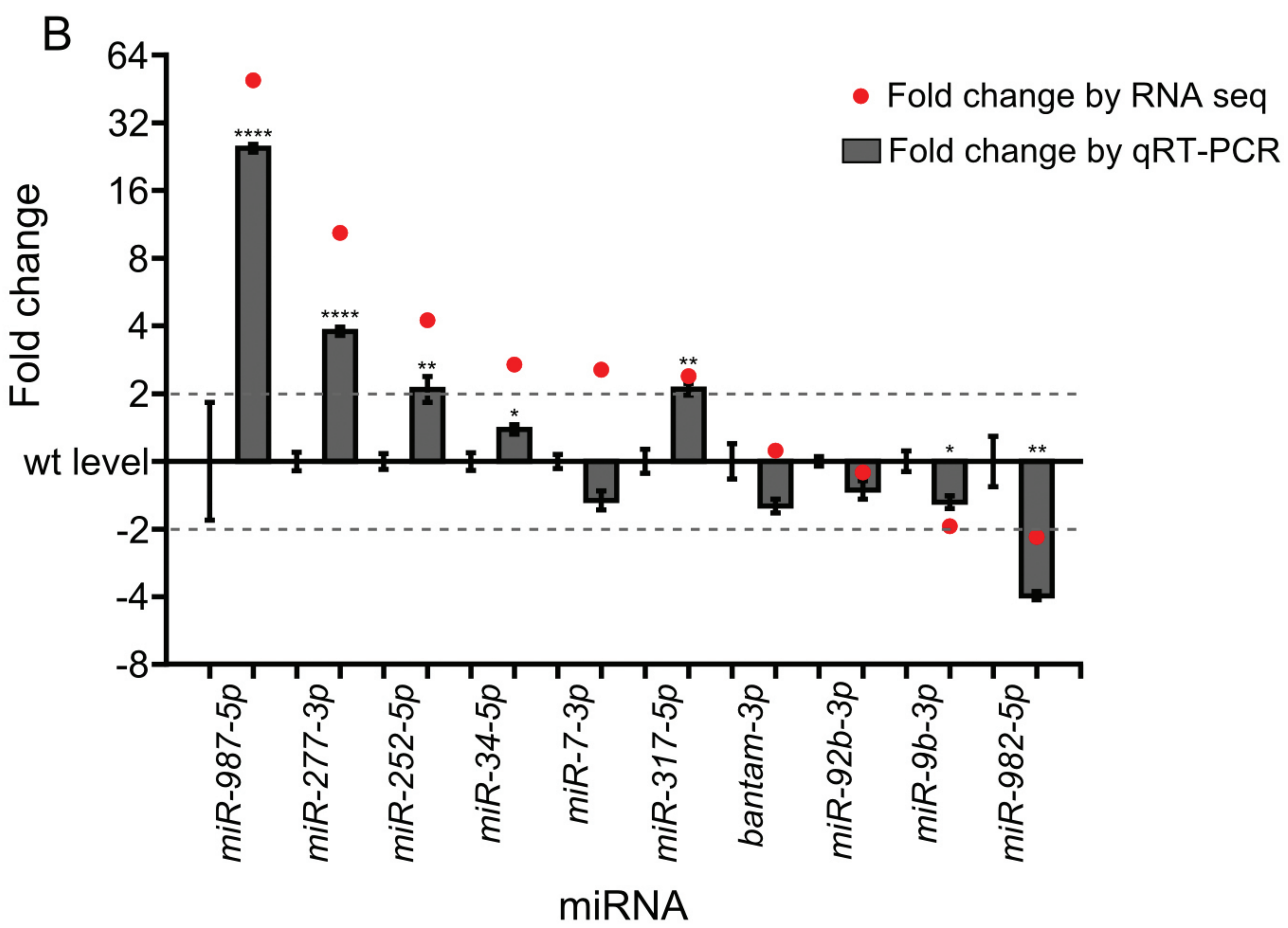
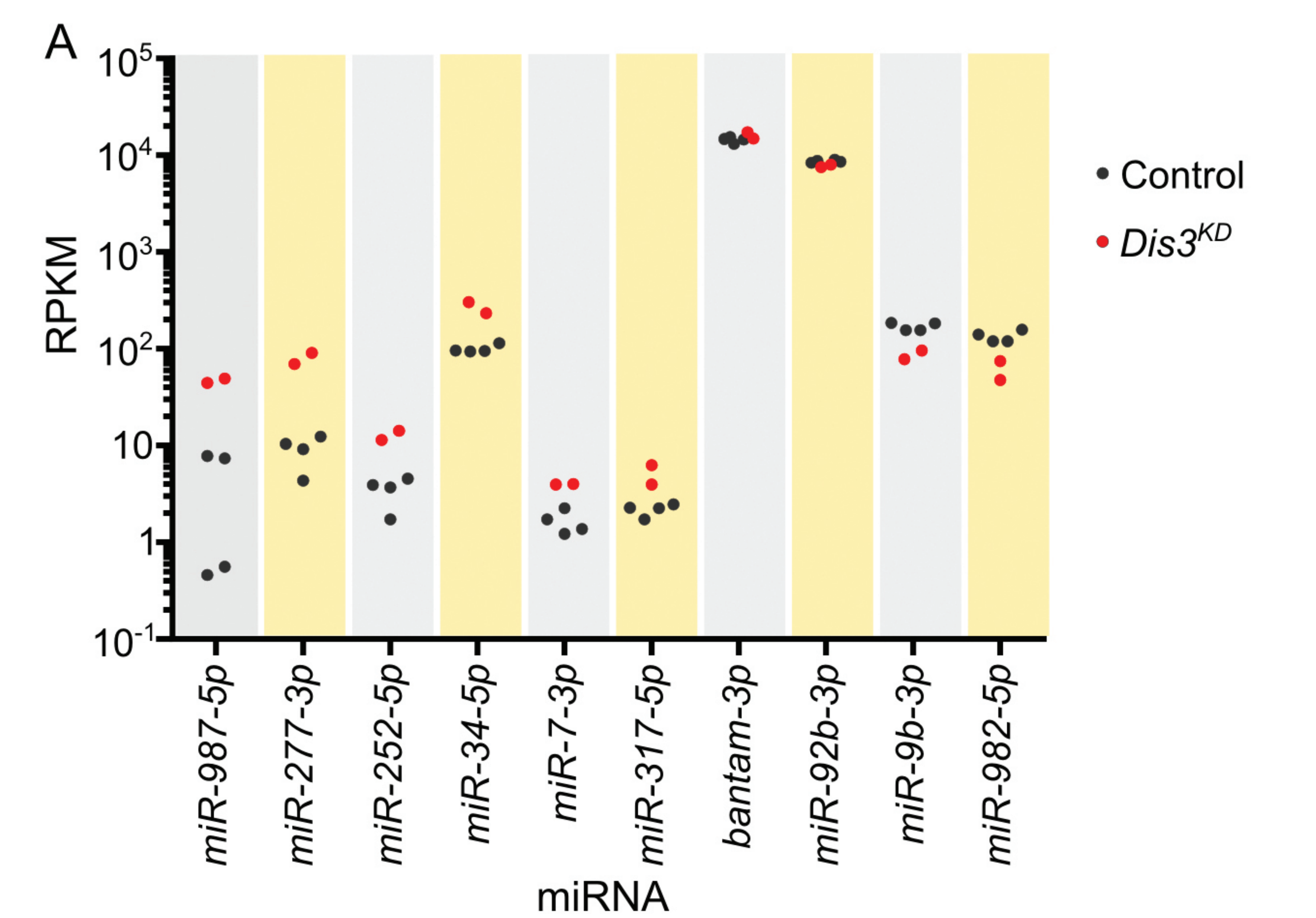




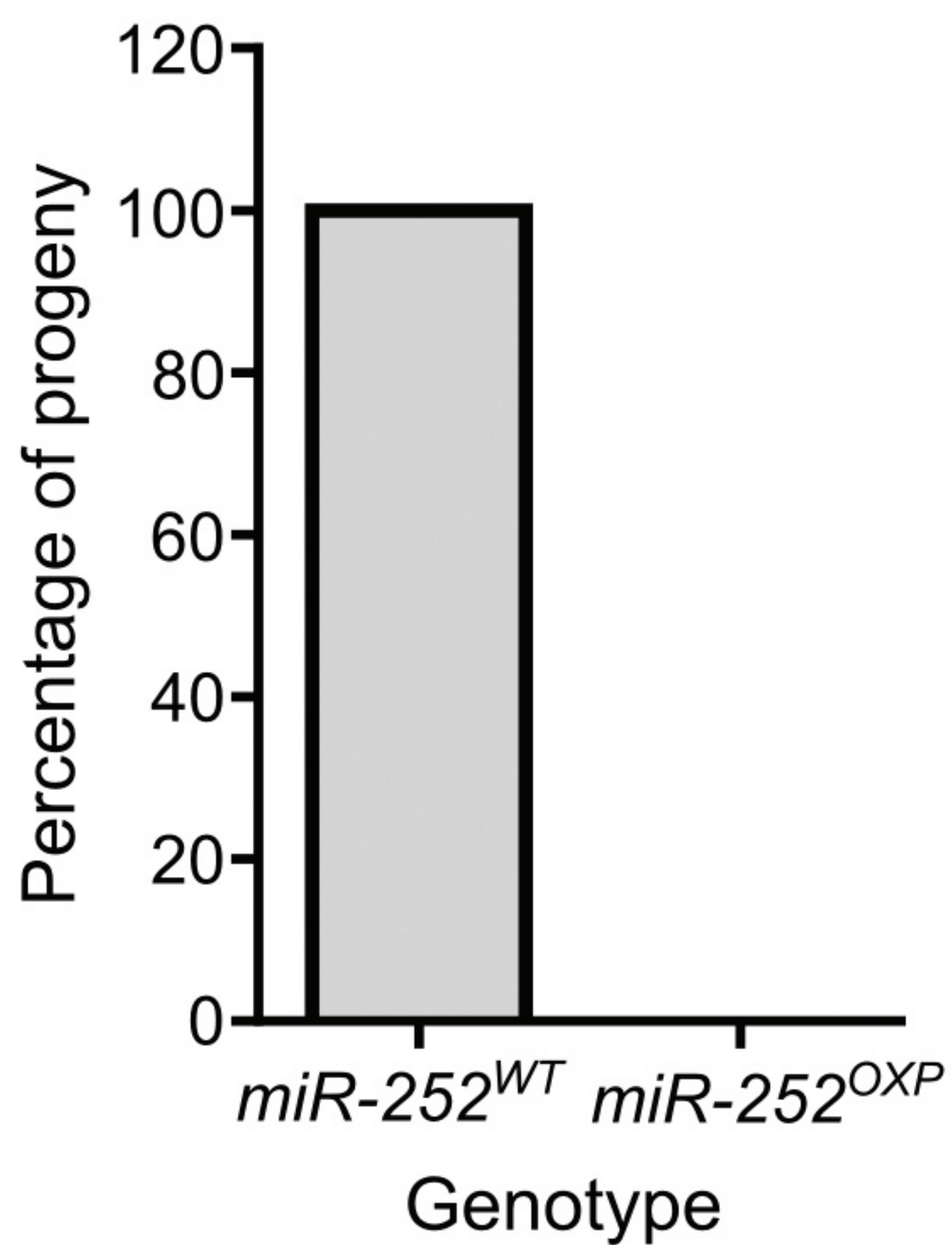




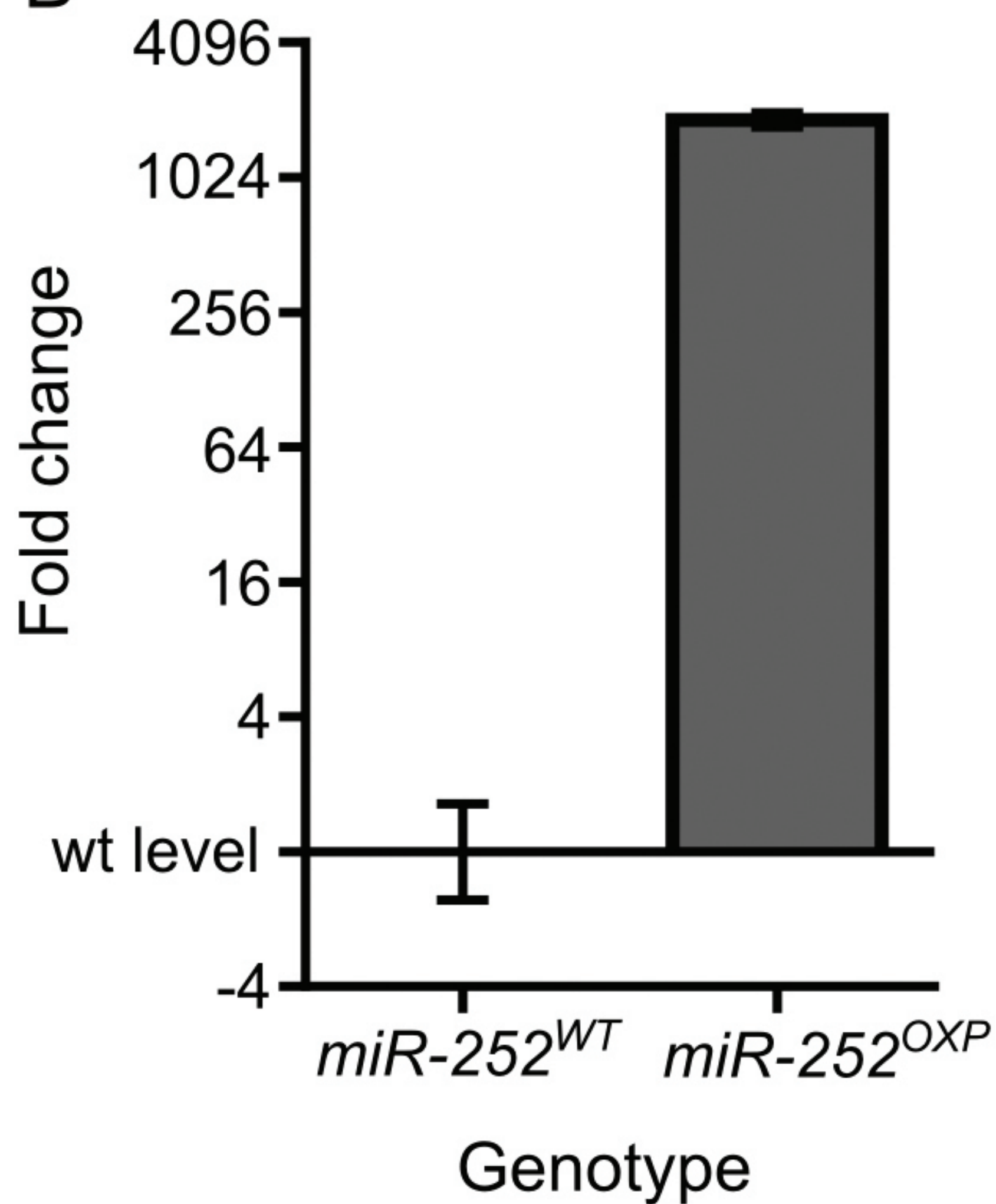
| | RNAseq read counts detected using miRDeep2 | | | | | | |
|----------------------------|--|------------|------------|------------|----------------------|----------------------|----------------------|
| | Parent 1-1 | Parent 1-2 | Parent 2-1 | Parent 2-2 | Dis3 ^{KD} 1 | Dis3 ^{KD} 2 | |
| Novel miR | 23 | 24 | 0 | 17 | 19 | 14 | |
| | qRT-PCR Cts | | | | | | |
| | Parent 1-1 | Parent 1-2 | Parent 2-1 | Parent 2-2 | Dis3 ^{KD} 1 | Dis3 ^{KD} 2 | Dis3 ^{KD} 3 |
| Novel miR | 31.7 | 32.3 | 31.5 | 31.4 | 31.4 | 31.6 | 31.5 |
| <i>snoR442</i> housekeeper | 22.1 | 22.6 | 22.3 | 22.4 | 21.5 | 21.6 | 21.7 |



A



B

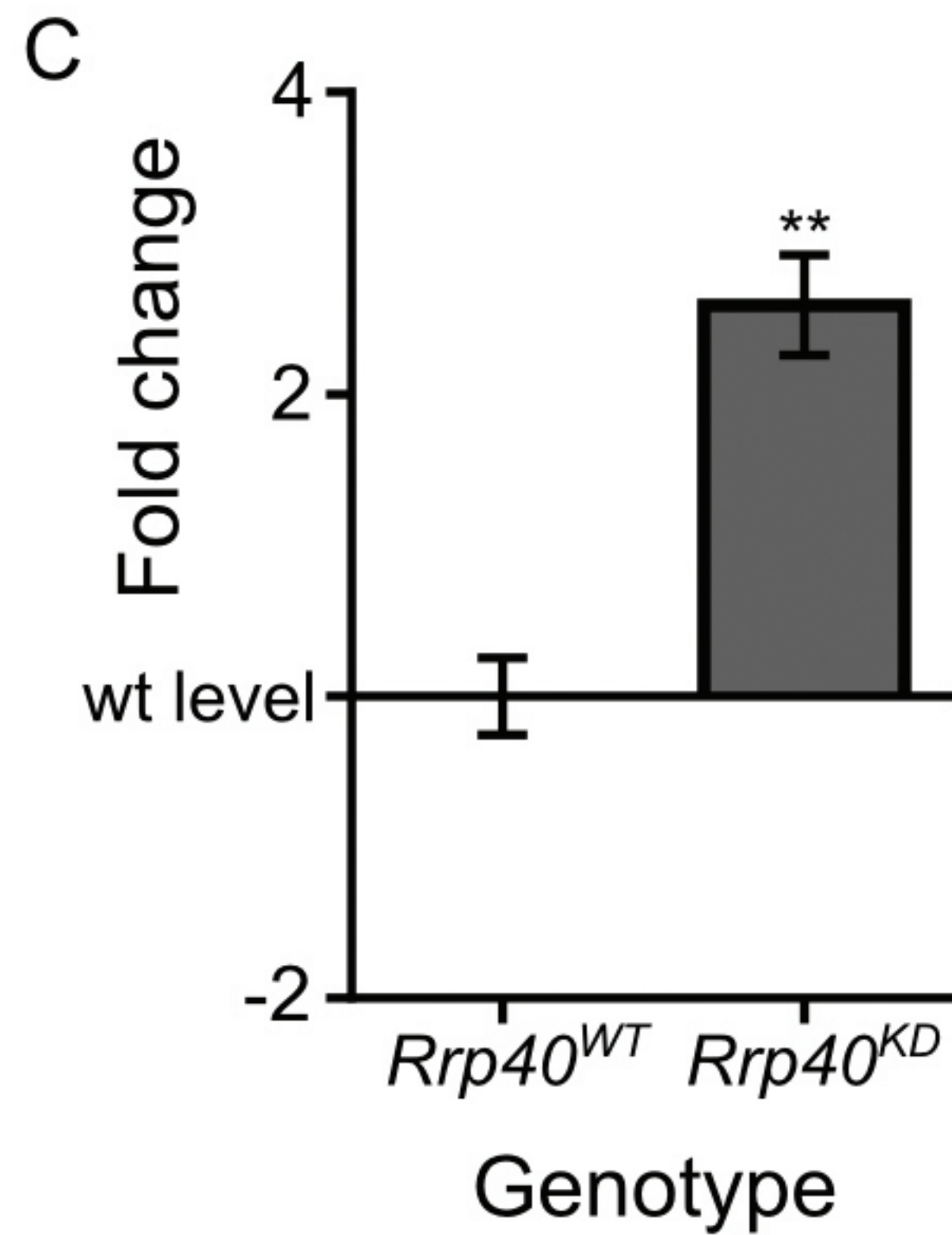


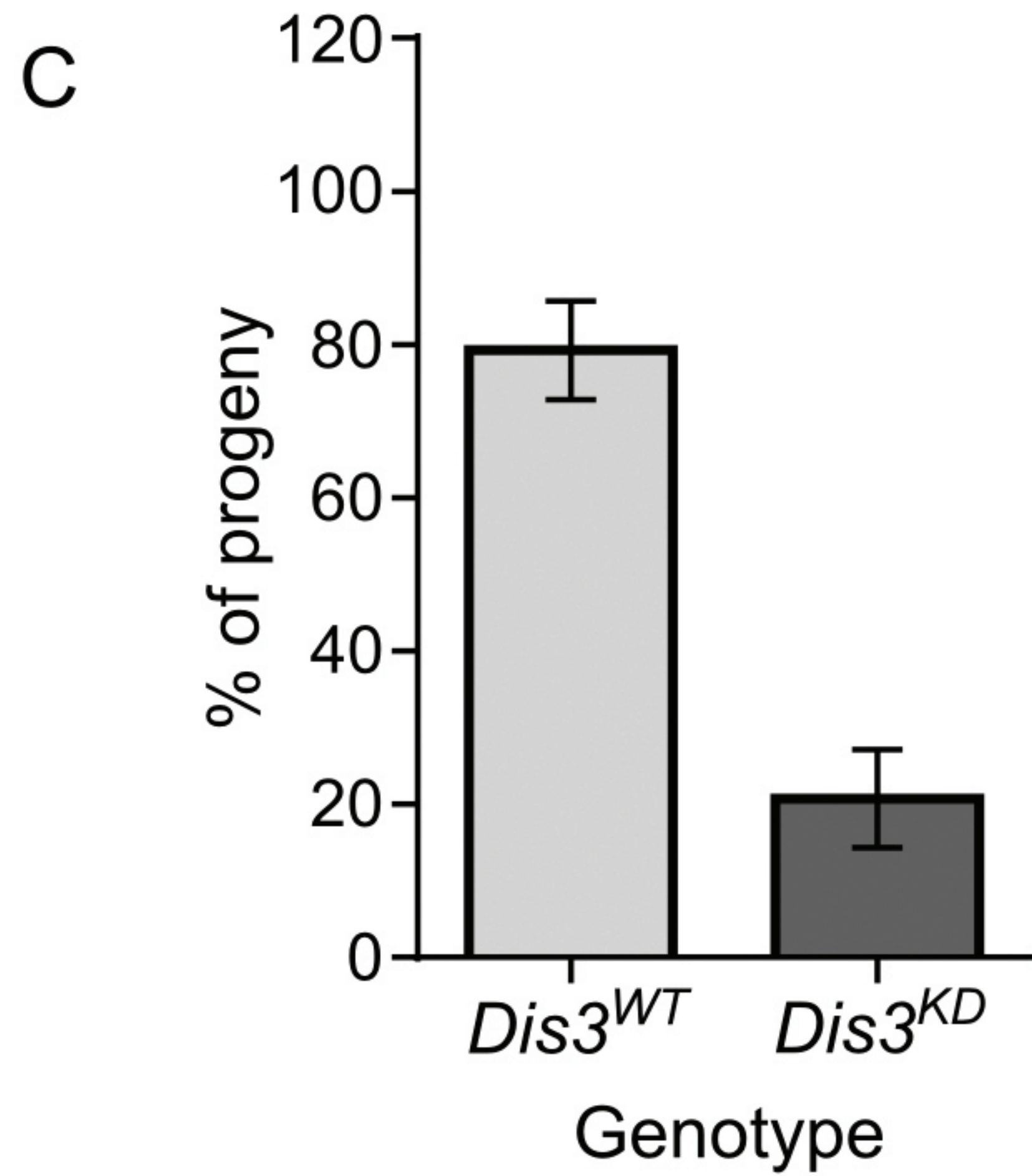
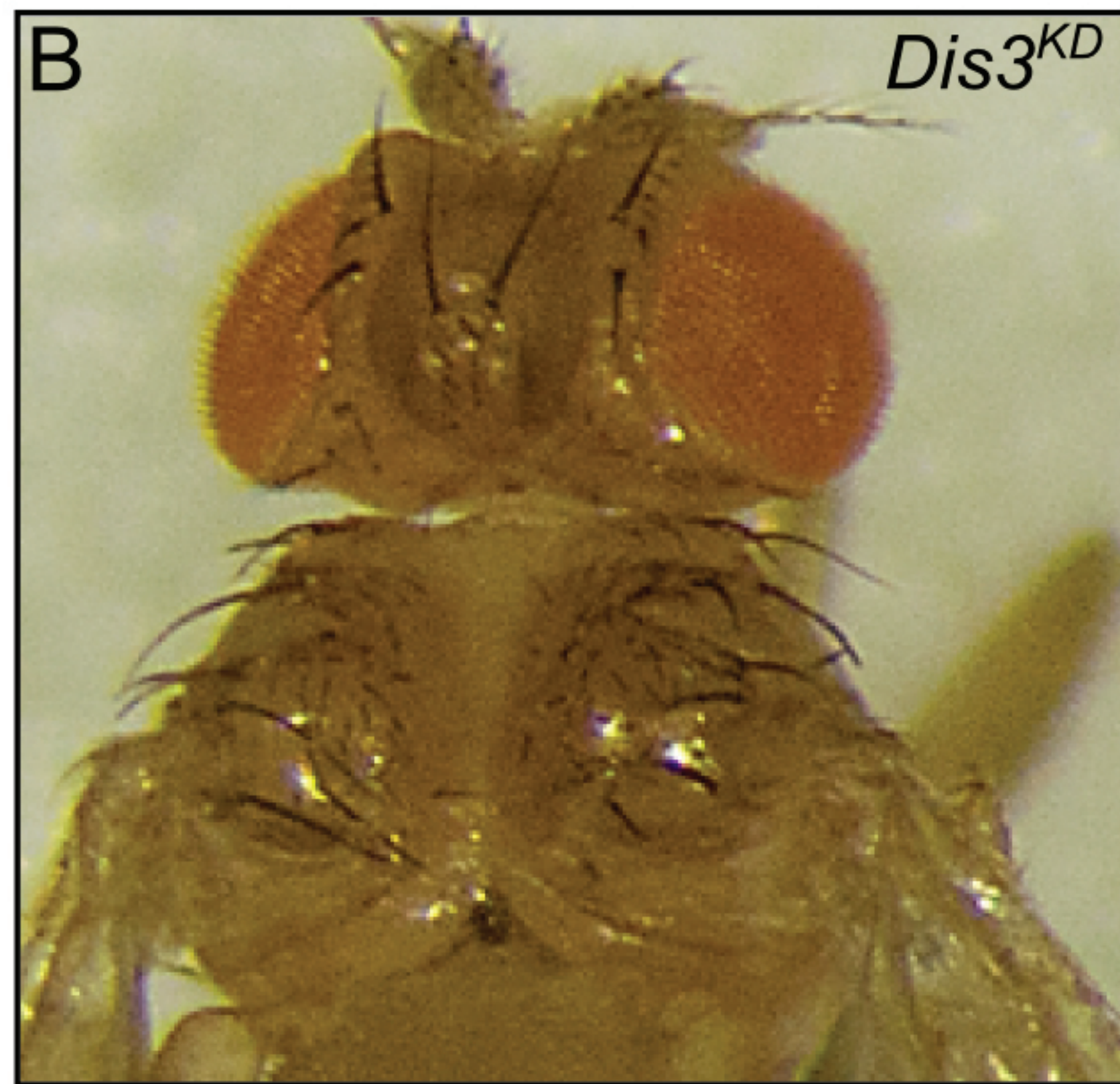
C

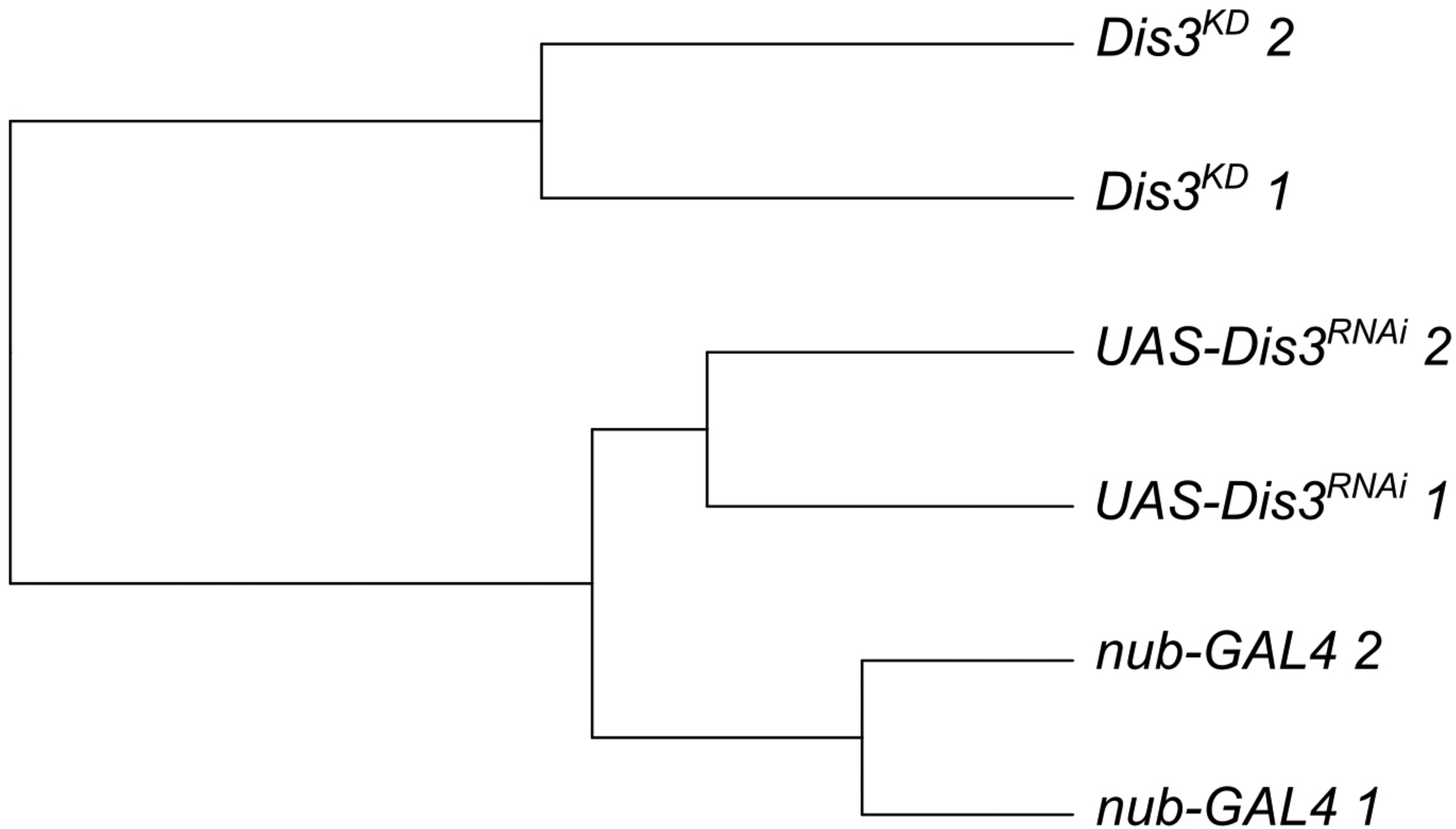


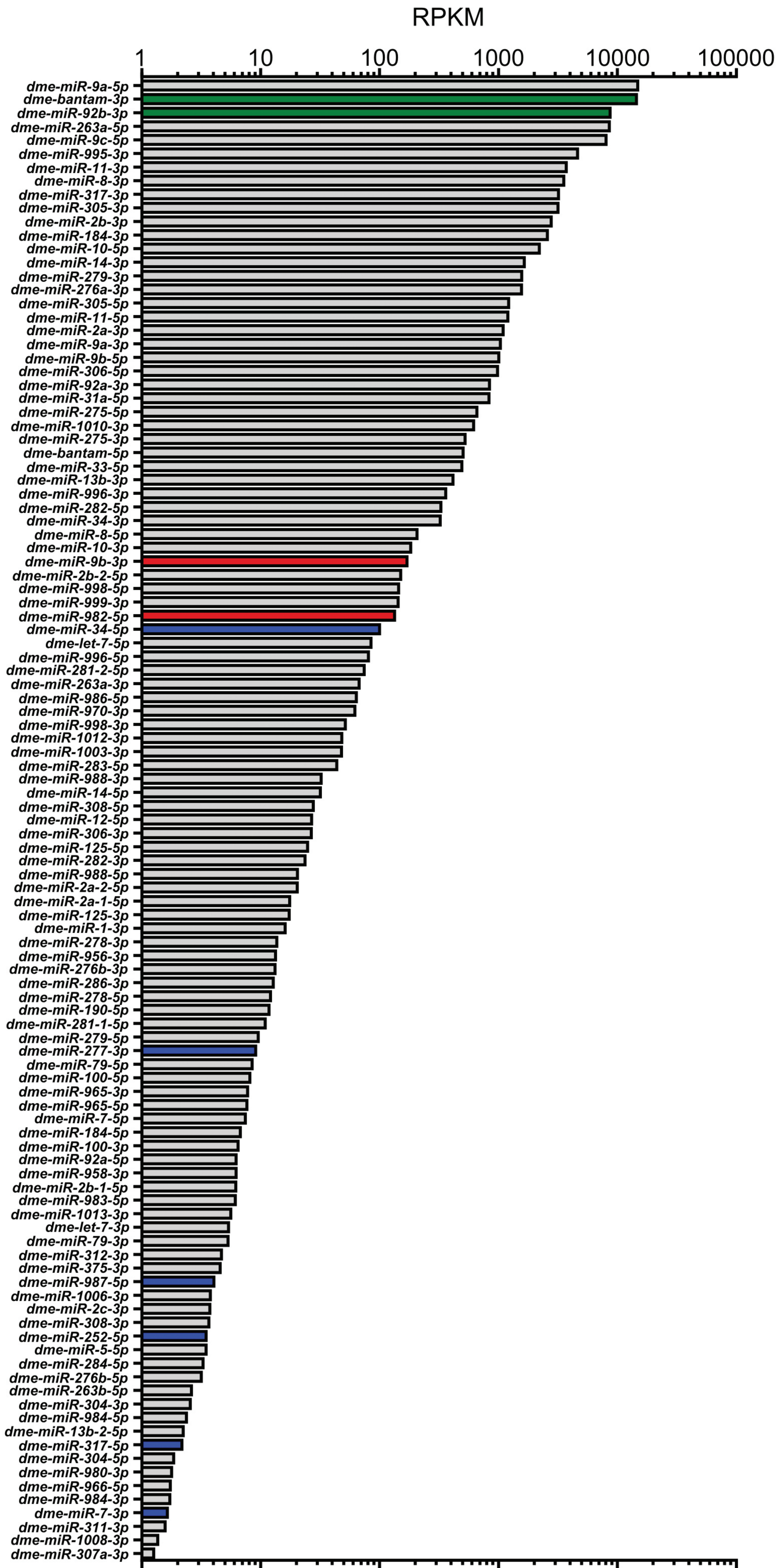
D











pre-miR-277 Forward: 5'-AGGTGAGTGTCTAGTGAAGCATCTA-3'

Probe: 5'-TAGTGTCTCCGTAAACTTTT-3'

Reverse: 5'-ACGAGAGAAACAGCTAGA-3'

pre-miR-987 Forward: 5'-TGTTGGACTGTGTTTAAAGTAAATAGTCTG-3'

Probe: 5'-CTCGAATGCAACTTTC-3'

Reverse: 5'-GCAGTTGAAGTAAATGCCTGTTGAT-3'

pre-miR-252 Forward: 5'-ACCAAGTTCGCTTTCCTAAGTACTAG-3'

Probe: 5'-TTGCGGACACGAACCTA-3'

Reverse: 5'-CTTGGGCAGCAGGAGGTA-3'

pre-miR-34 Forward: 5'-AGTGTGGTTAGCTGGTTGTGTAG-3'

Probe: 5'-CAACGGCAATAATTG-3'

Reverse: 5'-AGTGAAGATAGTGGCTGTGAATTGT-3'

pre-miR-317 Forward: 5'-ACCCTGTGCTCGCTTTGAA-3'

Probe: 5'-CACTTGCTTGCAATTCA-3'

Reverse: 5'-CAAACGGCCACTGGATACCA-3'

pre-miR-982 Forward: 5'-CGAAATCATGTTAGATCCTGGACAAAT-3'

Probe: 5'-AAGTAATTGATGCATAAAAAC-3'

Reverse: 5'-GCTCTAAAACCATTTAGTTCAAGGATGAA-3'

pre-miR-9b Forward: 5'-TGCATATTATTTGCTCTTTGGTGATTTTAG-3'

Probe: 5'-CTGTATGGTGTTTATGTATATTC-3'

Reverse: 5'-TGCAGAAACCATTTGGTTTTTGGTA-3'